On the rotating nonlinear Klein-Gordon equation: non-relativistic limit and numerical methods

Norbert Mauser, Yong Zhang, Xiaofei Zhao

ON THE ROTATING NONLINEAR KLEIN-GORDON EQUATION: NON-RELATIVISTIC LIMIT AND NUMERICAL METHODS

NORBERT J. MAUSER, YONG ZHANG, AND XIAOFEI ZHAO

Abstract. We consider numerics / asymptotics for the rotating nonlinear Klein-Gordon (RKG) equation, an important PDE in relativistic quantum physics that can model a rotating galaxy in Minkowski metric and serves also as a model e.g. for a "cosmic superfluid". Firstly, we formally show that in the non-relativistic limit RKG converges to coupled rotating nonlinear Schrödinger equations (RNLS), which is used to describe the particle-antiparticle pair dynamics. Investigations of the vortex state of RNLS are carried out. Secondly, we propose three different numerical methods to solve RKG from relativistic regimes to non-relativistic regimes in polar and Cartesian coordinates. In relativistic regimes, a semi-implicit finite difference Fourier spectral method is proposed in polar coordinates where both rotation terms are diagonalized simultaneously. While in non-relativistic regimes, to overcome the fast temporal oscillations, we adopt the rotating Lagrangian coordinates and introduce two efficient multiscale methods with uniform accuracy, i.e., the multi-revolution composition method and the exponential integrator. Various numerical results confirm (uniform) accuracy of our methods. Simulations of vortices dynamics are presented.

Keywords: Rotating nonlinear Klein-Gordon equation, cosmological models, non-relativistic limit, rotating two-component BEC, quantized vortex, numerical methods

AMS Subject Classification: 65M06, 65M70, 65Z99, 81Q05,85A40

1. Introduction

The universe has been modelled as a "superfluid" since the pioneering work of Witten [57] and Zurek [58]. Such superfluids [37] are often described by a complex-valued scalar field as Ginzburg and Landau proposed an order parameter for the phase coherence [26]. The nonlinear Klein-Gordon equation has then become a popular superfluid model, which is able to cover the entire velocity range, especially the relativistic region [28, 55, 31, 39, 53, 54, 15, 48, 23, 49, 21, 52]. As a model for describing a rotating galaxy in Minkowski metric, the nonlinear Klein-Gordon equation in a rotating frame [28, 31, 39, 53, 54] is used. Also, the nonlinear Klein-Gordon equation appears as a relativistic generalization of the Gross-Pitaevskii equation, a nonlinear Schrödinger equation that serves as a basic model for Bose-Einstein Condensates [2], also in the rotating case, see e.g. [2, 59, 50].

From these applications we motivate the following RKG equation that we study in this work :

$$\frac{1}{c^2}\partial_{tt}\Psi(\mathbf{x},t) - \Delta\Psi(\mathbf{x},t) + \left(\frac{mc}{\hbar}\right)^2 \Psi(\mathbf{x},t) + \left(V(\mathbf{x}) + m\lambda|\Psi(\mathbf{x},t)|^2\right)\Psi(\mathbf{x},t) - R_{Co} - R_{ce} = 0, \quad (1.1)$$

where the Coriolis term R_{Co} and the centrifugal term R_{ce} read as

$$R_{Co} = i\frac{2\Omega}{c^2}L_z\partial_t\Psi(\mathbf{x},t), \quad R_{ce} = \frac{\Omega^2}{c^2}L_z^2\Psi(\mathbf{x},t), \qquad t>0,$$

and $\mathbf{x} = (x,y) \in \mathbb{R}^2$ or $\mathbf{x} = (x,y,z) \in \mathbb{R}^3$, L_z is the z-component of the angular momentum operator:

$$L_z = -i\hbar(x\partial_y - y\partial_x),$$

$V(\mathbf{x}) : \mathbb{R}^d \to \mathbb{R}, d = 2, 3$ is an external trapping potential and $\Psi = \Psi(\mathbf{x},t) : \mathbb{R}^d \times \mathbb{R}^+ \to \mathbb{C}$ is the scaler field. The first order angular momentum operator term R_{Co} describes the Coriolis force and the second order angular term R_{ce} describes the centrifugal force in the rotation. The parameter c is the speed of light, $\hbar$ is the Plank constant, m denotes the mass, λ is the self-interaction constant and Ω denotes the angular velocity.

Equation (1.1) has been used to describe the creation and dynamics of the quantized vortices of a galaxy in 2D or 3D models as a "cosmic rotating superfluid". The vortices generation that obeys the relativistic Feynman relation, quantum turbulence in the form of a vortex tangle that follows mechanism for matter creation during the big bang era, and the formation and transmission of Kelvin waves correspond well to observations [28, 31, 39, 53, 54]. For generalisations of (1.1) to curved spacetime Klein-Gordon models, e.g. the BTZ metric or the Kerr metric for a black-hole, we refer to [15, 48, 49, 21, 52].

In order to adimensionalize the RKG equation we introduce the rescaling

$$\tilde{\mathbf{x}} = \frac{\mathbf{x}}{x_s}, \quad \tilde{t} = \frac{t}{t_s}, \quad \tilde{\Psi}(\tilde{\mathbf{x}}, \tilde{t}) = \Psi(\mathbf{x}, t), \quad t_s = \frac{m x_s^2}{\hbar}, \tag{1.2}$$

where t_s is the dimensionless time unit and x_s is the length unit, and denote

$$\varepsilon := \frac{\hbar}{mcx_s}, \quad \tilde{\Omega} = \Omega m x_s^2, \quad \tilde{\lambda} = \lambda m x_s^2, \quad \tilde{V}(\tilde{\mathbf{x}}) = x_s^2 V(\mathbf{x}), \quad \tilde{L}_z = -i(\tilde{x}\partial_{\tilde{y}} - \tilde{y}\partial_{\tilde{x}}).$$

Plugging (1.2) into (1.3), the dimensionless rotating nonlinear Klein-Gordon (RKG) equation (removing all the ˜ for simplicity) reads as follows

$$\varepsilon^2 \partial_{tt}\Psi - \Delta\Psi + \frac{1}{\varepsilon^2}\Psi + \left(V + \lambda|\Psi|^2\right)\Psi - 2i\Omega\varepsilon^2 L_z \partial_t \Psi - \Omega^2 \varepsilon^2 L_z^2 \Psi = 0, \quad \mathbf{x} \in \mathbb{R}^d, \ t > 0, \tag{1.3}$$

with $V = V(\mathbf{x})$, $\Psi = \Psi(\mathbf{x}, t)$.

The small dimensionless parameter ε tends to 0 as $\hbar \to 0$, the "(semi)classical" limit or/and as $c \to \infty$, the "non-relativistic" or "post-Newtonian" limit. Whereas the semiclassical limit of RKG is not yet achieved (preliminary work on the linear KG case is ongoing [1], the "non-relativistic limit" of nonlinear KG to Schrödinger type equations is quite well understood, see e.g. [14, 42, 43]. The combined limit from Dirac-Maxwell and KG-Maxwell to Vlasov-Poisson has been given in [45]. The large mass limit of the RKG has been considered in [55].

In this paper we fix $\hbar$ and consider $\varepsilon \to 0$ as the non-relativistic limit $c \to \infty$ and use (1.3) with the usual initial conditions [3, 4, 13, 42, 43, 47, 22]:

$$\Psi(\mathbf{x}, 0) = \psi_0(\mathbf{x}), \quad \partial_t \Psi(\mathbf{x}, 0) = \frac{1}{\varepsilon^2}\psi_1(\mathbf{x}), \quad \mathbf{x} \in \mathbb{R}^d, \tag{1.4}$$

where $\psi_0\,, \psi_1$ are complex-valued functions uniformly bounded (with respect to ε) in some Sobolev space. The RKG system (1.3)-(1.4) conserves the (*Hamiltonian*) *energy*

$$E(t) := \int_{\mathbb{R}^d} \Big(\varepsilon^2|\partial_t\Psi|^2 + |\nabla\Psi|^2 + \frac{1}{\varepsilon^2}|\Psi|^2 + V|\Psi|^2 + \frac{\lambda}{2}|\Psi|^4 - \Omega^2\varepsilon^2|L_z\Psi|^2\Big)d\mathbf{x} \equiv H(0), \ t \geq 0, \tag{1.5}$$

and the *charge*

$$Q(t) := \frac{i\varepsilon^2}{2}\int_{\mathbb{R}^d} \left(\Psi\partial_t\overline{\Psi} - \overline{\Psi}\partial_t\Psi + 2\Omega\Psi(x\partial_y - y\partial_x)\overline{\Psi}\right) d\mathbf{x}, \quad t \geq 0. \tag{1.6}$$

It is known [9] that the nonlinear Klein-Gordon equation with focusing self-interaction ($\lambda < 0$) can show possible finite time blow-up, whereas for the defocusing case ($\lambda > 0$) existence of the global solution is assured. Our discussion in this work is away from the critical blow-up time.

In this paper, we shall study the dynamics of the RKG (1.3) for a wide range of $\varepsilon \in (0, 1]$ and propose numerical methods for solving (1.3). We shall firstly apply formal analysis to show that the RKG (1.3) converges as $\varepsilon \to 0$ to a coupled nonlinear rotating Schrödinger equations (RNLS). We discuss the links between the RKG model and the RNLS, where the latter is a classical model for the rotating two-component Bose-Einstein Condensates [46, 36, 29, 30, 35]. Quantized vortices lattices will be obtained from the RNLS by minimizing the energy, and we shall then investigate numerically their dynamics in the RKG. In order to efficiently study the dynamics, we propose numerical methods for solving (1.3) in polar or Cartesian coordinates. The polar coordinates are popular for studying vortices dynamics in Schrödinger equation or Ginzburg-Landau equation in the literature [2, 6, 34, 12, 53, 28, 59]. We shall present a semi-implicit Fourier spectral method in the polar coordinates for the RKG, which simultaneously diagonalizes both rotating terms. In Cartesian coordinates, we aim to overcome the fast temporal oscillation in the solution of (1.3) as

$\varepsilon \ll 1$ and simulate efficiently the transition of the RKG in the non-relativistic limit. To do so, we introduce a rotating Lagrangian coordinates transform [8] to (1.3), which helps to eliminate the two rotating terms. Then the state-of-art multiscale methods with uniform discretization accuracy for all $\varepsilon \in (0, 1]$ will be applied for solving (1.3), including the multi-revolution composition method [19] and the exponential integrator [13]. In the end, we apply the presented methods to study the vortices dynamics in the RKG (1.3) for $\varepsilon \in (0, 1]$. Compared to the results in the Schrödinger models [6, 7, 41, 10], relativistic corrections to the vortices dynamics are clearly observed.

The paper is organized as follows. In section 2, we analyze the limit of the RKG as $\varepsilon \to 0$ and study the limit model. Numerical methods are proposed in section 3. Numerical tests and simulations are reported in section 4. Finally, some conclusions are drawn in section 5. We shall adopt the notation $A \lesssim B$ to represent that there exists a constant $C > 0$ which is independent of ε, such that $|A| \leq CB$.

2. Non-relativistic limit

By considering $0 < \varepsilon \ll 1$ in (1.3) in the sense of speed of light c going to infinity, we are in the non-relativistic limit regime of the cosmic rotating superfluid where only quantum effects remain. By formal analysis, we shall show that RKG converges to two-component Gross-Pitevskii type equations describing twp-component Bose-Einstein condensates (BEC) in the limit $\varepsilon \to 0$.

2.1. **Formal analysis.**

Assume that the solution of (1.3) satisfy an expansion [5, 3]:

$$\Psi(\mathbf{x}, t) = \mathrm{e}^{it/\varepsilon^2} z_+(\mathbf{x}, t) + \mathrm{e}^{-it/\varepsilon^2} \overline{z_-}(\mathbf{x}, t) + r(\mathbf{x}, t), \quad \mathbf{x} \in \mathbb{R}^d,\ t \geq 0, \tag{2.1}$$

where $z_\pm = z_\pm(\mathbf{x}, t)$ and $r = r(\mathbf{x}, t)$ are unknowns to be determined. Note that the fast oscillating phase factors correspond to the rest energy, like in the Foldy-Wouthousen transform for the non-relativistic limit of the Dirac equation (see e.g. [44]). Plugging (2.1) into the equation (1.3), we get

$$\begin{aligned}
&\mathrm{e}^{is/\varepsilon^2} \left[2i\partial_t - \Delta + V + \lambda(|z_+|^2 + 2|z_-|^2) + 2\Omega L_z\right] z_+ \\
&+ \mathrm{e}^{-is/\varepsilon^2} \left[-2i\partial_t - \Delta + V + \lambda(|z_-|^2 + 2|z_+|^2) - 2\Omega L_z\right] \overline{z_-} \\
&+ \varepsilon^2 \partial_{tt} r - \Delta r + \frac{r}{\varepsilon^2} + \mathrm{e}^{3it/\varepsilon^2} z_+^2 z_- + \mathrm{e}^{-3it/\varepsilon^2} \overline{z_-}^2 \overline{z_+} + \varepsilon^2 f_+ + \varepsilon^2 f_- + f_r = 0,
\end{aligned}$$

where

$$\begin{aligned}
f_+ =& \mathrm{e}^{it/\varepsilon^2} \left(\partial_{tt} - 2i\Omega L_z \partial_t - \Omega^2 L_z^2\right) z_+, \quad f_- = \mathrm{e}^{-it/\varepsilon^2} \left(\partial_{tt} - 2i\Omega L_z \partial_t - \Omega^2 L_z^2\right) \overline{z_-}, \\
f_r =& \mathrm{e}^{it/\varepsilon^2} \lambda \left(2z_+|r|^2 + z_- r^2\right) + \mathrm{e}^{-it/\varepsilon^2} \lambda \left(2\overline{z_-}|r|^2 + \overline{z_+} r^2\right) + \mathrm{e}^{2it/\varepsilon^2} \lambda \left(z_+^2 \overline{r} + 2z_+ z_- r\right) \\
&+ \mathrm{e}^{-2it/\varepsilon^2} \lambda \left(\overline{z_-}^2 \overline{r} + 2\overline{z_+ z_-} r\right) + 2\lambda(z_+ \overline{z_- r} + |z_+|^2 r + |z_-|^2 r + |r|^2 r) + Vr.
\end{aligned}$$

We can decompose the RKG equation into a pair of coupled Schrödinger equations:

$$\begin{cases} 2i\partial_t z_+ - \Delta z_+ + V z_+ + \lambda(|z_+|^2 + 2|z_-|^2) z_+ + 2\Omega L_z z_+ = 0, \\ 2i\partial_t z_- - \Delta z_- + V z_- + \lambda(|z_-|^2 + 2|z_+|^2) z_- + 2\Omega L_z z_- = 0, \end{cases} \tag{2.2}$$

and an equation for the reminder :

$$\varepsilon^2 \partial_{tt} r - \Delta r + \frac{r}{\varepsilon^2} + \mathrm{e}^{3it/\varepsilon^2} z_+^2 z_- + \mathrm{e}^{-3it/\varepsilon^2} \overline{z_-}^2 \overline{z_+} + \varepsilon^2 f_+ + \varepsilon^2 f_- + f_r = 0. \tag{2.3}$$

Based on the ansatz (2.1) and the initial condition (1.4), we have at $t = 0$

$$\begin{cases} z_+(\mathbf{x}, 0) + \overline{z_-}(\mathbf{x}, 0) + r(\mathbf{x}, 0) = \psi_0(\mathbf{x}), \\ \dfrac{i}{\varepsilon^2} \left[z_+(\mathbf{x}, 0) - \overline{z_-}(\mathbf{x}, 0)\right] + \partial_t z_+(\mathbf{x}, 0) + \partial_t \overline{z_-}(\mathbf{x}, 0) + \partial_t r(\mathbf{x}, 0) = \dfrac{\psi_1(\mathbf{x})}{\varepsilon^2}. \end{cases}$$

If we consider (2.2) associated with initial values

$$z_+(\mathbf{x}, 0) = \frac{1}{2} \left(\psi_0(\mathbf{x}) - i\psi_1(\mathbf{x})\right), \quad z_-(\mathbf{x}, 0) = \frac{1}{2} \left(\overline{\psi_0}(\mathbf{x}) - i\overline{\psi_1}(\mathbf{x})\right), \tag{2.4}$$

it leaves

$$r(\mathbf{x}, 0) = 0, \quad \partial_t r(\mathbf{x}, 0) = -\partial_t z_+(\mathbf{x}, 0) - \partial_t z_-(\mathbf{x}, 0).$$

When $\varepsilon \to 0$, the RKG (1.3) converges to the two coupled nonlinear Schrödinger equations with angular momentum rotation (2.2) and initial values (2.4), which is guaranteed by the following estimate:

Lemma 2.1. *Under the regularity assumption $\psi_0(\mathbf{x}), \psi_1(\mathbf{x}), V(\mathbf{x}) \in H^{m_0+4}(\mathbb{R}^d)$, $m_0 > d/2$, we have*

$$\|r(\cdot,t)\|_{H^{m_0}} \lesssim \varepsilon^2, \quad 0 \le t \le T, \tag{2.5}$$

for some $T > 0$ independent of ε.

Proof. Based on the assumption, we have directly $z_\pm(\mathbf{x},0) \in H^{m_0+4}(\mathbb{R}^d)$. Note $L_z = -i\partial_\theta$ and denote $\mathcal{L} = -\Delta - 2i\Omega\partial_\theta$. Then for the Schrödinger system (2.7), we have

$$z_\pm(\mathbf{x},t) = \mathrm{e}^{it/2\mathcal{L}} z_\pm(\mathbf{x},0) + \frac{i}{2}\int_0^t \mathrm{e}^{i(t-s)/2\mathcal{L}} \left[V(\mathbf{x}) + \lambda(|z_\pm(\mathbf{x},s)|^2 + 2|z_\mp(\mathbf{x},s)|^2)\right] z_\pm(\mathbf{x},s) ds.$$

Since $\mathrm{e}^{it/2\mathcal{L}}$ is bounded, then by the formal bootstrap argument, we have

$$\partial_t^k z_\pm(\mathbf{x},t) \in L^\infty((0,T); H^{m_0+4-2k}(\mathbb{R}^d)), \quad k = 0,1,2,$$

for some $T > 0$. It is then straightforward to see

$$f_\pm(\mathbf{x},t) \in L^\infty((0,T); H^{m_0}(\mathbb{R}^d)).$$

For the remainder's equation:

$$\begin{cases} \varepsilon^2 \partial_{tt} r - \Delta r + \dfrac{r}{\varepsilon^2} + \mathrm{e}^{3it/\varepsilon^2} z_+^2 z_- + \mathrm{e}^{-3it/\varepsilon^2} \overline{z_-}^2 \overline{z_+} + \varepsilon^2 f_+ + \varepsilon^2 f_- + f_r = 0, \\ r(\mathbf{x},0) = 0, \quad \partial_t r(\mathbf{x},0) = -\partial_t z_+(\mathbf{x},0) - \partial_t z_-(\mathbf{x},0), \end{cases}$$

we have by Duhamel's formula in Fourier space,

$$\begin{aligned} \widehat{r}(\xi,t) =& \frac{\sin(\omega_\xi t)}{\omega_\xi} \widehat{(\partial_t r)}(\xi,0) - \int_0^t \frac{\sin(\omega_\xi(t-\theta))}{\varepsilon^2\omega_\xi} \left[\varepsilon^2 \widehat{f}_+(\xi,\theta) + \varepsilon^2 \widehat{f}_-(\xi,\theta) + \widehat{f}_r(\xi,\theta)\right] d\theta, \\ & - \int_0^t \frac{\sin(\omega_\xi(t-\theta))}{\varepsilon^2\omega_\xi} \left[\mathrm{e}^{3i\theta/\varepsilon^2} \widehat{(z_+^2 z_-)}(\xi,\theta) + \mathrm{e}^{-3i\theta/\varepsilon^2} \widehat{(\overline{z_-^2 z_+})}(\xi,\theta)\right] d\theta, \quad \xi \in \mathbb{R}^d, \end{aligned} \tag{2.6}$$

with $\omega_\xi = \frac{1}{\varepsilon^2}\sqrt{1+\varepsilon^2|\xi|^2}$. Defining

$$\int_0^t \frac{\sin(\omega_\xi(t-\theta))}{\varepsilon^2\omega_\xi} \mathrm{e}^{3i\theta/\varepsilon^2} d\theta = \frac{\varepsilon^2\omega_\xi(\mathrm{e}^{3it/\varepsilon^2} - \cos(\omega_\xi t)) - 3i\sin(\omega_\xi t)}{\omega_\xi(\varepsilon^4\omega_\xi^2 - 9)} =: \varphi(\xi,t),$$

we have

$$\varphi(\xi) = O(\varepsilon^2), \quad |\xi| \le 2\varepsilon^{-1}.$$

Therefore in (2.6) for $|\xi| \le 2\varepsilon^{-1}$ we use an integration-by-parts argument to write, e.g. (same to the rests)

$$\begin{aligned} \int_0^t \frac{\sin(\omega_\xi(t-\theta))}{\varepsilon^2\omega_\xi} \mathrm{e}^{3i\theta/\varepsilon^2} \widehat{(z_+^2 z_-)}(\xi,\theta) d\theta =& \varphi(\xi,t) \widehat{(z_+^2 z_-)}(\xi,t) - \varphi(\xi,0) \widehat{(z_+^2 z_-)}(\xi,0) \\ & - \int_0^t \varphi(\xi,\theta) \widehat{(\partial_t (z_+^2 z_-))}(\xi,\theta) d\theta, \quad |\xi| \le 2\varepsilon^{-1}. \end{aligned}$$

With the Parserval's identity, we get from (2.6) for $0 \le t \le T$,

$$\begin{aligned} & \|r(\cdot,t)\|_{H^{m_0}} \\ & \lesssim \varepsilon^2 \|\partial_t r(\cdot,0)\|_{H^{m_0}} + \int_0^t \varepsilon^2 \left(\|f_+(\cdot,\theta)\|_{H^{m_0}} + \|f_-(\cdot,\theta)\|_{H^{m_0}}\right) d\theta + \int_0^t \|f_r(\cdot,\theta)\|_{H^{m_0}} d\theta \\ & + \varepsilon^2(1+t)\left(\|z_+\|_{L^\infty((0,T);H^{m_0})} + \|\partial_t z_+\|_{L^\infty((0,T);H^{m_0})} + \|z_-\|_{L^\infty((0,T);H^{m_0})} + \|\partial_t z_-\|_{L^\infty((0,T);H^{m_0})}\right) \\ & + \int_0^t \left(\|z_+^2 z_-(\cdot,\theta) - P_\varepsilon(z_+^2 z_-)(\cdot,\theta)\|_{H^{m_0}} + \|z_-^2 z_+(\cdot,\theta) - P_\varepsilon(z_-^2 z_+)(\cdot,\theta)\|_{H^{m_0}}\right) d\theta, \end{aligned}$$

with P_ε the projection operator

$$P_\varepsilon f(\mathbf{x},t) := \int_{|\xi|\le 2\varepsilon^{-1}} \widehat{f}(\xi,t)\mathrm{e}^{2\pi i\mathbf{x}\cdot\xi}d\xi.$$

It is clear to have

$$\|z_+^2 z_-(\cdot,t) - P_\varepsilon(z_+^2 z_-)(\cdot,t)\|_{H^{m_0}} \lesssim \varepsilon^2\|z_+^2 z_-(\cdot,t)\|_{H^{m_0+2}} \lesssim \varepsilon^2.$$

So we get

$$\|r(\cdot,t)\|_{H^{m_0}} \lesssim \varepsilon^2 + \int_0^t \|f_r(\cdot,\theta)\|_{H^{m_0}}d\theta, \quad 0\le t\le T.$$

Noting that $f_r = O(r)$, we get by using the bootstrap argument

$$\|r(\cdot,t)\|_{H^{m_0}} \lesssim \varepsilon^2, \quad 0<t\le T',$$

for some $0<T'\le T$ independent of ε. □

2.2. **The limit system.** As shown in Lemma 2.1, the limit system of the RKG when $\varepsilon\to 0$ is the rotating coupled nonlinear Schrödinger equation (RNLS) given below

$$\begin{cases} 2i\partial_t z_+ - \Delta z_+ + Vz_+ + \lambda(|z_+|^2+2|z_-|^2)z_+ + 2\Omega L_z z_+ = 0, \quad \mathbf{x}\in\mathbb{R}^d,\ t>0,\\ 2i\partial_t z_- - \Delta z_- + Vz_- + \lambda(|z_-|^2+2|z_+|^2)z_- + 2\Omega L_z z_- = 0,\\ z_+(\mathbf{x},0) = \dfrac{1}{2}\left(\psi_0(\mathbf{x}) - i\psi_1(\mathbf{x})\right), \quad z_-(\mathbf{x},0) = \dfrac{1}{2}\left(\overline{\psi_0}(\mathbf{x}) - i\overline{\psi_1}(\mathbf{x})\right). \end{cases} \tag{2.7}$$

The gap between RKG and RNLS is $O(\varepsilon^2)$. Indeed, the limit system RNLS reads similarly as the rotating two-component Bose-Einstein condensates (BEC) [46, 36, 29, 30, 35, 41, 50]. Lemma 2.1 gives a formal justification from the rotating Klein-Gordon model for cosmic superfluid to the rotating two-component BEC model through the non-relativistic limit. Rigorous mathematical analysis could also be done similarly as shown in [42, 43, 47].

The RNLS conserves the *mass* or the L^2-norm of each component

$$M_\pm(t) := \int_{\mathbb{R}^d} |z_\pm|^2 d\mathbf{x} \equiv M_\pm(0), \quad t\ge 0, \tag{2.8}$$

and the (*Hamiltonian*) *energy*

$$\begin{aligned} E_{nls}(t) :=& \frac{1}{2}\int_{\mathbb{R}^2}\left(|\nabla z_+|^2 + |\nabla z_-|^2 + V|z_+|^2 + V|z_-|^2 + \frac{\lambda}{2}(|z_+|^4 + |z_-|^4 + 2|z_+|^2|z_-|^2)\right)d\mathbf{x}\\ &- \Omega\int_{\mathbb{R}^d} Re\left(\overline{z}_+ L_z z_+ + \overline{z}_- L_z z_-\right)d\mathbf{x} \equiv E_{nls}(0), \quad t\ge 0. \end{aligned} \tag{2.9}$$

The charge conservation of RKG transits to mass conservation of RNLS through the limit $\varepsilon\to 0$. In fact, plugging the expansion (2.1) into the charge (1.6), we have

$$Q(t) = \int_{\mathbb{R}^d}\left(|z_+|^2 - |z_-|^2\right)d\mathbf{x} + O(\varepsilon^2).$$

The mass conservations (2.8) imply that $\|z_+\|_{L^2}^2 - \|z_-\|_{L^2}^2$ is a time-independent quantity which acts as the leading order approximation of the charge Q in the non-relativistic limit. According to the Dirac's hole theory or quantum field theory, z_+ represents *(normal) particles* with positive charge and z_- represents *antiparticles* with negative charge [16, 56]. Solving the limit model (2.7) serves as a valid approximation to the original problem in the regime $0<\varepsilon\ll 1$ [24].

The ground state of (2.7) can be defined as the minimizer of the energy functional (2.9) under constraints: $M_\pm = 1$. For (2.7), we have the same existence result of the ground state as the classical rotating BEC [2]: when the trapping potential is chosen as a harmonic function, i.e. $V = \frac{1}{2}\left(\gamma_x^2 x^2 + \gamma_y^2 y^2\right)$ with $\gamma_x>0, \gamma_y>0$ being the trapping frequency in x, y direction respectively, then the ground state of (2.7) exists if $|\Omega|<\Omega_c$ and $\lambda>-\lambda_c$, for some critical values $\Omega_c, \lambda_c>0$. We refer the readers to [2] for more details and a thorough study on the ground states of the two-component system (2.7) will be addressed in a coming work.

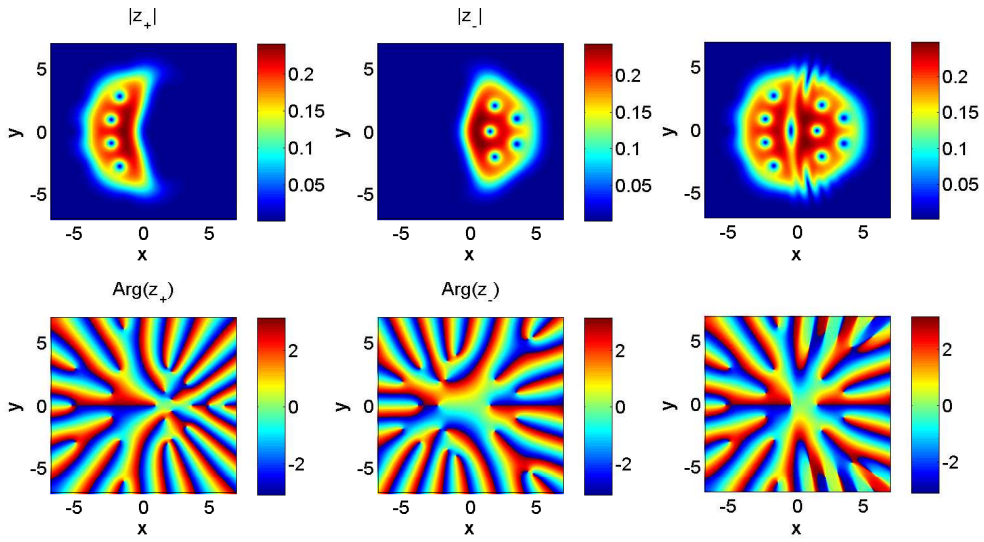

FIGURE 1. Contour plot of the bound state of the particle $z_+(\mathbf{x})$ (left), antiparticle $z_-(\mathbf{x})$ (middle) and the quantization $z_+(\mathbf{x}) + \overline{z}_-(\mathbf{x})$ (right) for $\omega = 0.9$.

The ground state under fast rotating speed contains quantized vortices which can be obtained numerically by the normalized gradient flow method [2]. It is clear that if one starts the gradient flow of the Hamiltonian E_{nls} from two identical states for the two components $z_\pm$, then in the ground state found by the algorithm, the two components would also be completely the same. To avoid this case, here we apply the normalized gradient flow to minimize the Hamiltonian starting from two different states:

$$z_+^0 = \frac{(1-\Omega)\phi_g(x,y) + \Omega\phi_g(x,y)(x-iy)}{\|(1-\Omega)\phi_g(x,y) + \Omega\phi_g(x,y)(x-iy)\|}, \quad z_-^0 = \overline{z_+^0},$$

where $\phi_g(x,y) := e^{-\frac{x^2+y^2}{2}}/\sqrt{\pi}$. This strategy will lead to a general bound state which is not necessarily a ground state. We shall use this bound state of the RNLS to produce a vortices pattern and later study its dynamics in the RKG for some $0 < \varepsilon \leq 1$.

Fig. 1 shows the bound state $z_+(\mathbf{x}), z_-(\mathbf{x})$ under $\lambda = 50$, $V = \frac{1}{2}(x^2+y^2)$ and $\Omega = 0.9$ found by the normalized gradient flow and $z_+(\mathbf{x}) + \overline{z}_-(\mathbf{x})$. In quantum field theory,

$$\mathrm{e}^{i\gamma} z_+ + \mathrm{e}^{-i\gamma}\overline{z_-}, \quad \gamma \in \mathbb{R},$$

gives the quantization of the field.

Compared with RKG, RNLS in general contains only the Coriolis force term, i.e. $L_z z_\pm$. The centrifugal force term R_{ce} in RKG, however, is a higher order perturbation in the non-relativistic limit regime, and it vanishes as $\varepsilon \to 0$. Therefore, by considering a wide range of $\varepsilon \in (0,1]$, one would expect to observe more interesting phenomena in RKG than in RNLS. That motivates us to consider a robust numerical solver for all $\varepsilon \in (0,1]$. The detailed relations between the two models are summarized in Tab. 1.

TABLE 1. Non-relativistic limit of the rotating Klein-Gordon equation.

$\varepsilon \to 0$	Rotating cosmic superfluid	Rotating two-component BEC
Model	Rotating nonlinear KG equation	Rotating coupled NLS equations
Angular term	Centrifugal term&Coriolis term	Coriolis term
Charge	Conserve charge (1.6)	Conserve Mass (2.8)
Energy	Conserve Hamiltonian (1.5)	Conserve Hamiltonian (2.9)

Remark 2.2. One can apply formal derivation and analysis to the rotating Klein-Gordon equation with more general power-law nonlinearity or higher order term. The resulting limit system would be modified with the corresponding generalized nonlinear terms.

3. Numerical methods

In this section, we propose numerical methods for computing the dynamics of RKG (1.3). We shall present efficient and accurate discretizations in polar coordinates and in the rotating Lagrangian coordinates in a sequel. For simplicity, we just illustrate numerical methods in 2D. Extensions to 3D are straightforward.

3.1. **Polar Coordinates.** It has been popular to simulate the quantized vortices dynamics on a disk-shaped domain in polar coordinates [2, 6, 12, 53, 28, 59, 34], where the angular momentum operator reads simply as derivative with respect to the angle, i.e. $L_z = -i\partial_\theta$. It is convenient to truncate the whole space problem onto a disk

$$\Omega_{R_0} := \left\{ \mathbf{x} \in \mathbb{R}^2 \big| |\mathbf{x}| \le R_0 \right\},$$

where the radius $R_0 > 0$ is large enough to hold the dynamics, and to impose homogenous Neumann boundary condition. In polar coordinates, (1.3) reads as follows

$$\varepsilon^2 \left(\partial_{tt} - 2\Omega \partial_{t\theta} + \Omega^2 \partial_{\theta\theta} \right) \Psi - \left(\partial_{rr} + \frac{1}{r}\partial_r + \frac{1}{r^2}\partial_{\theta\theta} \right) \Psi + \frac{1}{\varepsilon^2}\Psi + \left(V + \lambda |\Psi|^2 \right) \Psi = 0, \tag{3.1}$$

with initial values and boundary conditions

$$\begin{aligned}
&\Psi(r,\theta,t=0) = \psi_0(r,\theta),\ \partial_t \Psi(r,\theta,t=0) = \frac{1}{\varepsilon^2}\psi_1(r,\theta), \quad 0 \le r \le R_0,\ 0 \le \theta \le 2\pi, \\
&\partial_r \Psi(R_0,\theta,t) = 0, \qquad |\Psi(0,\theta,t)| < \infty \quad t \ge 0,\ 0 \le \theta \le 2\pi, \\
&\Psi(r,0,t) = \Psi(r,2\pi,t), \quad \partial_\theta \Psi(r,0,t) = \partial_\theta \Psi(r,2\pi,t), \quad t \ge 0,\ 0 \le r \le R_0.
\end{aligned}$$

Semi-implicit finite difference Fourier spectral method. We present a semi-implicit finite difference Fourier spectral (**SIFS**) method to solve (3.1). Firstly, thanks to the periodicity in θ, we approximate the wave function Ψ by a truncated Fourier series, i.e.

$$\Psi(r,\theta) \approx \sum_{k=-N_\theta/2}^{N_\theta/2-1} \widehat{\Psi}_k(r)\ e^{ik\theta}, \quad \theta \in [0, 2\pi], \tag{3.2}$$

with N_θ being an even integer. The Fourier coefficient $\widehat{\Psi}_k(r)$ is defined and approximated as

$$\widehat{\Psi}_k(r) = \frac{1}{2\pi}\int_0^{2\pi} \Psi(r,\theta) e^{-ik\theta} d\theta \approx \frac{1}{N_\theta} \sum_{j=0}^{N_\theta - 1} \Psi\left(r, j\Delta\theta\right)\ e^{-ikj\Delta\theta},$$

with $\Delta\theta = \frac{2\pi}{N_\theta}$. Plugging (3.2) into (3.1), we have for $k = -N_\theta/2, \ldots, N_\theta/2 - 1$,

$$\varepsilon^2 \left(\partial_{tt} - 2\Omega\ ik\partial_t - \Omega^2 k^2 \right) \widehat{\Psi}_k = \left(\partial_{rr} + \frac{1}{r}\partial_r - \frac{k^2}{r^2} \right) \widehat{\Psi}_k - \frac{1}{\varepsilon^2}\widehat{\Psi}_k + \widehat{(F(\Psi))}_k, \quad 0 \le r < R_0, \tag{3.3}$$

with $F(\Psi) = -(V + \lambda|\Psi|^2)\Psi$. Notice that all θ-derivatives terms are diagonalized explicitly. However, diagonalising the operators in r-direction is not so simple. One may consider to use the Laguerre polynomials as basis [7], but then there are no fast transform algorithms. Consequently, the state-of-art time integrators which evaluate the stiff linear part exactly *can not* be applied in an efficient way. Hence, to evolve (3.3) from time $t_n := n\Delta t$ to t_{n+1} by a time step $\Delta t > 0$, it is more convenient to apply a classical three-level semi-implicit finite difference scheme as follows

$$\varepsilon^2(\delta_t^2 - 2\Omega\ ik\delta_t - \Omega^2 k^2 \mu_t)\widehat{\Psi}_k^n = \left(\partial_{rr} + \frac{1}{r}\partial_r - \frac{k^2}{r^2} - \frac{1}{\varepsilon^2} \right) \widehat{(\mu_t \Psi^n)}_k + \widehat{(F(\Psi^n))}_k, \quad n \ge 1, \tag{3.4}$$

where Ψ^n is the numerical approximation of $\Psi(\cdot, t_n)$, and

$$\delta_t \Psi^n = \frac{\Psi^{n+1} - \Psi^{n-1}}{2\Delta t}, \quad \delta_t^2 \Psi^n = \frac{\Psi^{n+1} - 2\Psi^n + \Psi^{n-1}}{(\Delta t)^2}, \quad \mu_t \Psi^n = \frac{1}{2}(\Psi^{n+1} + \Psi^{n-1}).$$

The semi-implicit treatment rewards us with unconditional stability [4]. (3.4) is numerically further discretized in r-direction by a second order finite difference method on a uniform mesh with a half-grid shift [38, 40]. We choose integer $N_r > 0$ and denote $r_j = (j-1/2)\Delta r$ with $\Delta r = R_0/N_r, j = 0, 1, \cdots, N_r+1$. The full discretization then reads:

$$\varepsilon^2(\delta_t^2 - 2\Omega\ ik\delta_t)\widehat{\Psi}^n_{k,j} = \left(\Delta_r - \frac{1}{\varepsilon^2} + \varepsilon^2\Omega^2k^2\right)\widehat{(\mu_t\Psi^n)}_{k,j} + \widehat{(F(\Psi^n))}_{k,j}, \quad n \geq 1, \tag{3.5}$$

for $k = -N_\theta/2, \ldots, N_\theta/2-1$, $j = 1, \ldots, N_r$. Here we define the discrete operator $\Delta_r\widehat{\Psi}^n_{k,j}$ as follows:

$$\Delta_r\widehat{\Psi}^n_{k,j} = \frac{\widehat{\Psi}^n_{k,j+1} - 2\widehat{\Psi}^n_{k,j} + \widehat{\Psi}^n_{k,j-1}}{(\Delta r)^2} + \frac{1}{r_j}\ \frac{\widehat{\Psi}^n_{k,j+1} - \widehat{\Psi}^n_{k,j-1}}{2\Delta r} - \frac{k^2}{r_j^2}\widehat{\Psi}^n_{k,j},\ j = 1, \ldots, N_r, \tag{3.6}$$

where $\widehat{\Psi}^n_{k,j}$ is an approximation of $\widehat{\Psi}^n_k(r_j)$. For the boundary values, i.e. $j = N_r+1$, the homogeneous Neumann boundary condition implies $\widehat{\Psi}^n_{k,N_r} = \widehat{\Psi}^n_{k,N_r+1},\ \forall n \in \mathbb{N}$. Using the half-grid shift grids, we *do not* have to deal with the singularity at $r = 0$ or imposing any boundary conditions thereof [38, 40]. To complete the scheme, the starting values can be obtained explicitly as $\Psi^0 = \psi_0$ and

$$\begin{aligned}\Psi^1 &= \Psi^0 + \Delta t\ \partial_t\Psi(\cdot, t=0) + \frac{(\Delta t)^2}{2}\ \partial_{tt}\Psi(\cdot, t=0)\\ &= \Psi^0 + \Delta t\ \frac{1}{\varepsilon^2}\ \psi_1 + \frac{(\Delta t)^2}{2}\ \partial_{tt}\Psi(\cdot, t=0),\end{aligned} \tag{3.7}$$

where $\partial_{tt}\Psi(\cdot, t=0)$ can be obtained explicitly by setting $t = 0$ in (3.1).

The SIFS scheme is semi-implicit, however, at each time level, it only requires a tri-diagonal linear solver, and it is quite simple with Thomas algorithm and cheap with $O(N_rN_\theta \log N_\theta)$ complexity. However, the finite difference integrator has under-resolution as ε becomes small. This can be seen by the error bound. Since the solution $\Psi(\mathbf{x}, t)$ propagates waves with wavelength $O(\varepsilon^2)$ in time which implies $\partial_{ttt}\Psi = O(\varepsilon^{-6})$, the error bound of SIFS up to a fixed time is

$$O\left(\frac{\Delta t^2}{\varepsilon^6}\right) + O(\Delta r^2) + O(\Delta\theta^{m_0}),$$

with some $m_0 > 0$ depends on the regularity of the solution in θ. Therefore, to obtain a correct approximation, one needs to adopt $\Delta t = O(\varepsilon^3)$, which brings heavy computational burden for $0 < \varepsilon \ll 1$ in the non-relativistic limit regime.

3.2. **Rotating Lagrangian coordinates.** To propose an efficient algorithm for solving (1.3) for a wide range of $\varepsilon \in (0, 1]$, we need to overcome the fast temporal oscillation of the solution in the non-relativistic limit by some multiscale integration methods. However, the Coriolis rotating term $2i\Omega\varepsilon^2L_z\partial_t\Psi$ and the centrifugal force term $\Omega^2\varepsilon^2L_z^2\Psi$ in the RKG equation prevents applications of the popular multiscale strategies like in [3, 17, 19, 13] to (1.3). Here, borrowing the idea of coordinates transform from the rotating BEC [41, 8], we introduce the rotating Lagrangian coordinates and perform a coordinates transform to (1.3).

We introduce the rotating matrix

$$A(t) := \begin{pmatrix}\cos(\Omega t) & \sin(\Omega t)\\ -\sin(\Omega t) & \cos(\Omega t)\end{pmatrix}, \quad t \geq 0,$$

and denote the unknown of the RKG (1.3) in the *rotating Lagrangian coordinates* as:

$$u(\tilde{\mathbf{x}}, t) = \Psi(\mathbf{x}, t), \quad \mathbf{x} = A(t)\tilde{\mathbf{x}}. \tag{3.8}$$

Directly we have

$$\begin{aligned}&\partial_t u = \nabla\Psi(\dot{A}\tilde{\mathbf{x}}) + \partial_t\Psi,\\ &\partial_{tt}u = (\dot{A}\tilde{\mathbf{x}})^T\nabla^2\Psi(\dot{A}\tilde{\mathbf{x}}) + \nabla\Psi(\ddot{A}\tilde{\mathbf{x}}) + 2\nabla\partial_t\Psi(\dot{A}\tilde{\mathbf{x}}) + \partial_{tt}\Psi.\end{aligned} \tag{3.9}$$

Noting that

$$\dot{A}\tilde{\mathbf{x}} = \Omega\begin{pmatrix}y\\ -x\end{pmatrix}, \quad \ddot{A}\tilde{\mathbf{x}} = -\Omega^2\mathbf{x}, \quad (\dot{A}\tilde{\mathbf{x}})^T\nabla^2\Psi(\dot{A}\tilde{\mathbf{x}}) = \Omega^2\left(x^2\partial_{yy}\Psi - 2xy\partial_{xy}\Psi + y^2\partial_{xx}\Psi\right),$$

(3.9) becomes

$$\partial_{tt}u = \Omega^2\left(x^2\partial_{yy}\Psi - 2xy\partial_{xy}\Psi + y^2\partial_{xx}\Psi - x\partial_x\Psi - y\partial_y\Psi\right) + 2\Omega(y\partial_{xt}\Psi - x\partial_{yt}\Psi) + \partial_{tt}\Psi.$$

Using the facts:

$$L_z\partial_t\Psi = i(y\partial_{xt}\Psi - x\partial_{yt}\Psi), \quad L_z^2\Psi = -x^2\partial_{yy}\Psi + 2xy\partial_{xy}\Psi - y^2\partial_{xx}\Psi + x\partial_x\Psi + y\partial_y\Psi,$$

we see

$$\partial_{tt}u = -\Omega^2 L_z^2\Psi - 2i\Omega L_z\partial_t\Psi + \partial_{tt}\Psi.$$

By further noting that

$$\Delta_{\tilde{\mathbf{x}}}u = \Delta\Psi,$$

we get the *RKG in the rotating Lagrangian coordinates*:

$$\varepsilon^2\partial_{tt}u(\tilde{\mathbf{x}},t) - \Delta u(\tilde{\mathbf{x}},t) + \frac{1}{\varepsilon^2}u(\tilde{\mathbf{x}},t) + \left[V(A(t)\tilde{\mathbf{x}}) + \lambda|u(\tilde{\mathbf{x}},t)|^2\right]u(\tilde{\mathbf{x}},t) = 0, \quad \tilde{\mathbf{x}}\in\mathbb{R}^2,\ t>0, \tag{3.10a}$$

$$u(\tilde{\mathbf{x}},0) = \psi_0(\tilde{\mathbf{x}}), \quad \partial_t u(\tilde{\mathbf{x}},0) = \Omega\nabla\psi_0(\tilde{\mathbf{x}})\begin{pmatrix}\tilde{y}\\-\tilde{x}\end{pmatrix} + \frac{1}{\varepsilon^2}\psi_1(\tilde{\mathbf{x}}), \quad \tilde{\mathbf{x}}\in\mathbb{R}^d, \tag{3.10b}$$

where the angular momentum terms have been eliminated and (3.10) is simply a nonlinear Klein-Gordon equation. When the trapping potential $V(\mathbf{x})$ is isotropic, i.e. $V(\mathbf{x}) = U(|\mathbf{x}|)$ for some function $U(\cdot):\mathbb{R}\to\mathbb{R}$, then $V(A(t)\tilde{\mathbf{x}}) = V(\tilde{\mathbf{x}})$ in (3.10), and the RKG in the rotating frame (3.10) is also an Hamiltonian system without external time dependence. We shall remove all the $\tilde{}$ in (3.10) in the following for simplicity.

For the numerical discrestization, we truncate the whole space problem (3.10) onto a bounded interval $I = (-a,a)\times(b,b)\in\mathbb{R}^2$ and impose approximately the periodic boundary conditions:

$$\varepsilon^2\partial_{tt}u(\mathbf{x},t) - \Delta u(\mathbf{x},t) + \frac{1}{\varepsilon^2}u(\mathbf{x},t) + \left[V(A(t)\mathbf{x}) + \lambda|u(\mathbf{x},t)|^2\right]u(\mathbf{x},t) = 0, \quad \mathbf{x}\in I,\ t>0, \tag{3.11a}$$

$$u(\mathbf{x},0) = \psi_0(\mathbf{x}), \quad \partial_t u(\mathbf{x},0) = \Omega\nabla\psi_0(\mathbf{x})\begin{pmatrix}y\\-x\end{pmatrix} + \frac{1}{\varepsilon^2}\psi_1(\mathbf{x}), \quad \mathbf{x}\in[-a,a]\times[-b,b], \tag{3.11b}$$

$$u(a,y,t) = u(-a,y,t), \quad \partial_x u(a,y,t) = \partial_x u(-a,y,t), \quad y\in[-b,b],\ t\geq 0, \tag{3.11c}$$

$$u(x,b,t) = u(x,-b,t), \quad \partial_y u(x,b,t) = \partial_y u(x,-b,t), \quad x\in[-a,a],\ t\geq 0. \tag{3.11d}$$

We consider (3.11) for a wide range of the "non-relativistic" parameter $0<\varepsilon\leq 1$. Since (3.11) reads as a standard cubic Klein-Gordon equation, many numerical methods in the literature could apply. Here to solve (3.11) with robustness on $0<\varepsilon\leq 1$, we shall consider two multiscale numerical integrators. One is the uniformly accurate (UA) exponential integrator (EI) and the other is the multi-revolution composition (MRC) method. MRC applies when $V(\mathbf{x})$ is isotropic and the scheme is geometric which provides good behaviour in long-time computing [19]. EI applies in general (anisotropic $V(\mathbf{x})$) and the scheme is optimal in computational cost [13]. Both methods give approximations with uniform accuracy for all $0<\varepsilon\leq 1$. That is to say the schemes can capture accurately the dynamics in the rotating cosmic superfluid and its transition to the rotating NLS in the non-relativistic limit under the same computational cost.

Multi-revolution composition method. The multi-revolution composition (MRC) method applies when the trapping potential in (3.11) is *isotropic*, so $V(A(t)\mathbf{x}) = V(\mathbf{x})$. The MRC method is originally proposed in [19] as a general geometric framework for autonomous highly oscillatory problems. It has been applied to solve oscillatory nonlinear Schrödinger equation [20] and recently to Vlasov equation [18]. Particularly in [18], MRC has been revealed to give uniform accuracy in terms of the oscillation frequency. We shall for the first time apply this method to solve the RKG by firstly perform a suitable reformulation of (3.11).

Introduce unknowns $w_\pm$:

$$w_+(\mathbf{x},t) := u(\mathbf{x},t) - i\varepsilon^2 A_\varepsilon\partial_t u(\mathbf{x},t), \quad w_-(\mathbf{x},t) := \overline{u}(\mathbf{x},t) - i\varepsilon^2 A_\varepsilon\partial_t\overline{u}(\mathbf{x},t), \tag{3.12}$$

and operators

$$A_\varepsilon := \frac{1}{\sqrt{1-\varepsilon^2\Delta}}, \quad D_\varepsilon := \frac{1}{\varepsilon^2}\left[\sqrt{1-\varepsilon^2\Delta} - 1\right].$$

Then the RKG (3.11) can be written as

$$i\partial_t w_\pm(\mathbf{x},t) = -\frac{1}{\varepsilon^2} w_\pm(\mathbf{x},t) + F_\pm(w_+(\mathbf{x},t), w_-(\mathbf{x},t)), \tag{3.13}$$

with

$$F_\pm(w_+, w_-) = -D_\varepsilon w_\pm - A_\varepsilon \left[\frac{\lambda}{8}\left|w_\pm + \overline{w}_\mp\right|^2 + \frac{V}{2}\right](w_\pm + \overline{w}_\mp).$$

It is clear to see that the pseudo-differential operators satisfy

$$0 < A_\varepsilon \le 1, \quad 0 \le D_\varepsilon \le -\frac{\Delta}{2}.$$

Suppose we are solving RKG (3.11) till time $T_f > 0$. Then by a rescaling of the time $t \to \varepsilon^2 t$, we rewrite(3.13) as

$$i\partial_t w_\pm(\mathbf{x},t) = -w_\pm(\mathbf{x},t) + \varepsilon^2 F_\pm(w_+(\mathbf{x},t), w_-(\mathbf{x},t)), \quad 0 < t \le \frac{T_f}{\varepsilon^2}, \tag{3.14a}$$

$$w_+(\mathbf{x},0) = u(\mathbf{x},0) - i\varepsilon^2 A_\varepsilon \partial_t u(\mathbf{x},0), \quad w_-(\mathbf{x},0) = \overline{u}(\mathbf{x},0) - i\varepsilon^2 A_\varepsilon \partial_t \overline{u}(\mathbf{x},0), \tag{3.14b}$$

on the periodic box $(-a,a)\times(-b,b)$ for $\mathbf{x}$.

Clearly, we see the linear part of (3.14) generates a 2π-periodic flow and the nonlinear part is bounded as $\varepsilon \to 0$. Now we write the final time as

$$\frac{T_f}{\varepsilon^2} = 2\pi M_f + T_r, \quad M_f = \frac{T_f}{2\pi\varepsilon^2} \in \mathbb{N}, \quad 0 \le T_r < 2\pi.$$

The 2nd order MRC method begins by choosing an integer $0 < M_0 \le M_f$ with

$$\alpha = \frac{1}{2}\left(1 + \frac{1}{M_0}\right), \quad \beta = \frac{1}{2}\left(1 - \frac{1}{M_0}\right), \quad N = \frac{M_f}{M_0}, \quad H = \varepsilon^2 M_0,$$

denoting $w_\pm^n \approx w_\pm(2\pi n M_0)$, and then the MRC scheme proceeds as

$$\begin{pmatrix} w_+^{n+1} \\ w_-^{n+1} \end{pmatrix} = \mathcal{E}_\beta(-2\pi)\mathcal{E}_\alpha(2\pi)\begin{pmatrix} w_+^{n} \\ w_-^{n} \end{pmatrix}, \quad 0 \le n \le N-1, \tag{3.15}$$

where $\mathcal{E}_\alpha(2\pi)$ denotes the flow:

$$i\partial_t w_\pm = -w_\pm + \alpha H F_\pm(w_+, w_-), \quad 0 < t \le 2\pi, \tag{3.16}$$

and $\mathcal{E}_\beta(-2\pi)$ denotes the flow:

$$i\partial_t w_\pm = -w_\pm - \beta H F_\pm(w_+, w_-), \quad -2\pi \le t < 0. \tag{3.17}$$

After evaluating (3.15) till $n = N$, the MRC method is completed by solving the remaining flow $\mathcal{E}_r(T_r)$:

$$i\partial_t w_\pm = -w_\pm + \varepsilon^2 F_\pm(w_+, w_-), \quad 0 < t \le T_r. \tag{3.18}$$

To further integrate the sub-flow (3.16), (3.17) or (3.18), we use a Strang splitting scheme. For example for $\mathcal{E}_\alpha(2\pi)$ (similarly for others):

$$i\partial_t w_\pm = (-1 - \alpha H D_\varepsilon) w_\pm - \alpha H A_\varepsilon \left[\frac{\lambda}{8}\left|w_\pm + \overline{w}_\mp\right|^2 + \frac{V}{2}\right](w_\pm + \overline{w}_\mp)$$

we split the flow as

$$\mathcal{E}_\alpha^k(t) : i\partial_t w_\pm = (-1 - \alpha H D_\varepsilon) w_\pm \quad \text{and} \quad \mathcal{E}_\alpha^p(t) : i\partial_t w_\pm = -\alpha H A_\varepsilon \left[\frac{\lambda}{8}\left|w_\pm + \overline{w}_\mp\right|^2 + \frac{V}{2}\right](w_\pm + \overline{w}_\mp).$$

Noting that $w_\pm + \overline{w}_\mp$ is time-independent in $\mathcal{E}_\alpha^k(t)$, both $\mathcal{E}_\alpha^k(t)$ and $\mathcal{E}_\beta^k(t)$ can be evaluated exactly. The exact solution of $\mathcal{E}_\alpha^k(t)$ is

$$w_\pm(\mathbf{x},t) = \mathrm{e}^{it(1+\alpha H D_\varepsilon)} w_\pm(\mathbf{x},0), \quad t > 0,$$

and the exact solution of $\mathcal{E}_\beta^p(t)$ is

$$w_\pm(\mathbf{x},t) = w_\pm(\mathbf{x},0) + it\alpha H A_\varepsilon \left[\frac{\lambda}{8}\left|w_\pm(\mathbf{x},0) + \overline{w}_\mp(\mathbf{x},0)\right|^2 + \frac{V}{2}\right](w_\pm(\mathbf{x},0) + \overline{w}_\mp(\mathbf{x},0)), \quad t > 0.$$

We take the same integer N to discretize the time interval $[0, 2\pi]$ of the subflow $\mathcal{E}_\alpha(2\pi)$ and denote the (micro) time step size as $h = 2\pi/N$. Then $\mathcal{E}_\alpha(2\pi)$ is approximated by the Strang splitting:

$$\mathcal{E}_\alpha(2\pi) \approx \left(\mathcal{E}_\alpha^p(h/2)\mathcal{E}_\alpha^k(h)\mathcal{E}_\alpha^p(h/2)\right)^N.$$

It is worth noting that when M_0 decreases to the critical value $M_0 = 1$, we have $\alpha = 1$, $\beta = 0$ in the MRC scheme and hence $\mathcal{E}_\beta(-2\pi)$ becomes identity. It means that MRC automatically reduces to direct integration on the flow (3.14) with the Strang splitting scheme under the time step $\Delta t = h$. Therefore, adopting the strategy proposed in [18], for some given integer $N > 0$ (the number of macro grids, which is the preferred user controlled parameter in practice) such that $M_0 = T_f/\varepsilon^2/(2\pi N) < 1$, we shall consider the MRC scheme as the direct Strang splitting scheme on (3.14) with time step $\Delta t = h = 2\pi/N$ accomplished by the remaining flow (3.18). With $w_\pm^n$ from the MRC scheme (3.15), one gets the numerical solution of RKG by

$$u(\mathbf{x}, t_n) \approx u^n = \frac{1}{2}\left(w_+^n + \overline{w}_-^n\right), \quad \partial_t u(\mathbf{x}, t_n) \approx u_t^n = \frac{i}{2\varepsilon^2 A_\varepsilon}\left(w_+^n - \overline{w}_-^n\right). \tag{3.19}$$

In practice, the involved spatial differentiations A_ε and D_ε in the MRC scheme could be computed by the Fourier pseudo-spectral discretization in the bounded space interval I under spatial step size $\Delta x, \Delta y > 0$.

The MRC framework is a geometric method which guarantees good long-time behavior of the method. Moreover, the proposed MRC scheme is charge-preserving.

Lemma 3.1. *The proposed MRC scheme (3.15)-(3.19) preserves the charge (1.6) of the RKG at the discrete time level in the Lagrangian coordinates.*

Proof. Under the coordinates change (3.8) and reformulation (3.12), the charge (1.6) in terms of the new variables in the Lagrange coordinates read as

$$Q(t) = \frac{1}{4}\int_{\mathbb{R}^2} \mathrm{Re}\left[(w_+(\mathbf{x}, t) + \overline{w_-}(\mathbf{x}, t))A_\varepsilon^{-1}(\overline{w_+}(\mathbf{x}, t) - w_-(\mathbf{x}, t))\right] d\mathbf{x}.$$

Note that the MRC scheme is a composition of sub-flows such as $\mathcal{E}_\alpha^k(t)$ and $\mathcal{E}_\beta^k(t)$, where the sub-flows are exactly integrated. Hence, the rest part of the proof is by directly checking that $\mathcal{E}_\alpha^k(t)$ and $\mathcal{E}_\beta^k(t)$ (same to the others) preserve the charge. □

Noting that the linear part of the flow in (3.14) is isometric, so provided that the solution of (3.14) is sufficiently smooth and using similar proof strategy in [20], the temporal error of the MRC method at a fixed time can be shown to have a super convergence in terms of ε, and the optimal total error bound thus reads:

$$O(H^2) + O(\varepsilon^2 h^2) + O(\Delta x^{m_0}) + O(\Delta y^{m_0}),$$

where $m_0 > 0$ depends on the smoothness of the solution in space. MRC is temporally second order accurate with respect to the number of macro time grid points N (noting $H, h = O(N^{-1})$) and spectrally accurate in space discretization.

UA exponential integrator. As another uniformly accurate (UA) method, the exponential integrator (EI) proposed in [13] for solving the nonlinear Klein-Gordon equation in the non-relativistic limit regime can be applied to handle *general potential* function V case, e.g. non-symmetric or time-dependent. The scheme is optimal in computational costs compared to the other UA methods [3, 17, 18]. The scheme gets very complicated at high order versions particularly when the solution of the Klein-Gordon equation is complex-valued. Here to study the vortices dynamics in (3.11), we need to consider complex-valued initial values ψ_0, ψ_1 for (3.11) in order to have non-zero charge. Therefore, to make an application of the EI scheme for (3.11), we write down the first order scheme under the complex-valued case with a brief derivation.

Based on (3.13), we further introduce the filtered variables

$$v_+(\mathbf{x}, t) := \mathrm{e}^{-it/\varepsilon^2}\left(u(\mathbf{x}, t) - i\varepsilon^2 A_\varepsilon \partial_t u(\mathbf{x}, t)\right), \quad v_-(\mathbf{x}, t) := \mathrm{e}^{-it/\varepsilon^2}\left(\overline{u}(\mathbf{x}, t) - i\varepsilon^2 A_\varepsilon \partial_t \overline{u}(\mathbf{x}, t)\right),$$

then the RKG (3.11) can be written as

$$i\partial_t v_\pm = -D_\varepsilon v_\pm - A_\varepsilon \mathrm{e}^{-it/\varepsilon^2}\left[\frac{\lambda}{8}\left|\mathrm{e}^{it/\varepsilon^2}v_\pm + \mathrm{e}^{-it/\varepsilon^2}\overline{v}_\mp\right|^2 + \frac{V(A(t)\mathbf{x})}{2}\right]\left(\mathrm{e}^{it/\varepsilon^2}v_\pm + \mathrm{e}^{-it/\varepsilon^2}\overline{v}_\mp\right).$$

By Duhamel's principle for some $n \geq 0$, one gets (drop $\mathbf{x}$ for simplicity)

$$\begin{aligned} v_\pm(t_{n+1}) = \frac{iA_\varepsilon}{8}\int_0^{\Delta t} \mathrm{e}^{i(\Delta t-\theta)D_\varepsilon - i(t_n+\theta)/\varepsilon^2}\lambda\left(\mathrm{e}^{i(t_n+\theta)/\varepsilon^2}v_\pm(t_n+\theta) + \mathrm{e}^{-i(t_n+\theta)/\varepsilon^2}\overline{v_\mp}(t_n+\theta)\right) \\ \times\left[4V(A(t_n+\theta)\mathbf{x}) + \left|\mathrm{e}^{i(t_n+\theta)/\varepsilon^2}v_\pm(t_n+\theta) + \mathrm{e}^{-i(t_n+\theta)/\varepsilon^2}\overline{v_\mp}(t_n+\theta)\right|^2\right]d\theta + \mathrm{e}^{i\Delta t D_\varepsilon}v_\pm(t_n). \end{aligned}$$

The first order scheme completes by approximating $A(t_n+\theta) \approx A(t_n)$, $v_\pm(t_n+\theta) \approx v_\pm(t_n)$ and then carrying out the integration exactly.

In details, denoting $v_\pm^n(\mathbf{x}) \approx v_\pm(\mathbf{x}, t_n)$, the EI scheme reads for $n \geq 0$,

$$\begin{aligned} v_\pm^{n+1} =& \mathrm{e}^{i\Delta t D_\varepsilon}v_\pm^n + \mathrm{e}^{2it_n/\varepsilon^2}c_1\lambda(v_\pm^n)^2 v_\mp^n + c_2\left[\lambda(|v_\pm^n|^2 + 2|v_\mp^n|^2) + 4V(A(t_n)\mathbf{x})\right]v_\pm^n \\ &+ \mathrm{e}^{-2it_n/\varepsilon^2}c_3\left[\lambda(|v_\mp^n|^2 + 2|v_\pm^n|^2) + 4V(A(t_n)\mathbf{x})\right]\overline{v_\mp^n} + \mathrm{e}^{-4it_n/\varepsilon^2}c_4\lambda\overline{v_\pm^n(v_\mp^n)^2}, \end{aligned} \tag{3.20}$$

with

$$\begin{aligned} c_1 &= \varepsilon^2 A_\varepsilon\frac{\mathrm{e}^{2i\Delta t/\varepsilon^2} - \mathrm{e}^{iD_\varepsilon\Delta t}}{16 - 8\varepsilon^2 D_\varepsilon}, \quad c_2 = A_\varepsilon\frac{\mathrm{e}^{iD_\varepsilon\Delta t} - 1}{8D_\varepsilon}, \\ c_3 &= \varepsilon^2 A_\varepsilon\frac{\mathrm{e}^{iD_\varepsilon\Delta t} - \mathrm{e}^{-2i\Delta t/\varepsilon^2}}{16 + 8D_\varepsilon\varepsilon^2}, \quad c_4 = \varepsilon^2 A_\varepsilon\frac{\mathrm{e}^{iD_\varepsilon\Delta t} - \mathrm{e}^{-4i\Delta t/\varepsilon^2}}{32 + 8D_\varepsilon\varepsilon^2} \end{aligned}$$

The approximation to the solution of RKG (3.11) would be

$$u(\mathbf{x}, t^n) \approx \frac{1}{2}\left[\mathrm{e}^{it_n/\varepsilon^2}v_+^n(\mathbf{x}) + \mathrm{e}^{-it_n/\varepsilon^2}\overline{v_-^n}(\mathbf{x})\right].$$

The above involved spatial differentiations could also be done by the Fourier discretization in space. Up to a fixed time, the error of the EI scheme (3.20) is

$$O(\Delta t) + O(\Delta x^{m_0}) + O(\Delta y^{m_0}).$$

4. Numerical results

In this section, we present the convergence results of the proposed numerical methods and the simulation results of the vortices dynamics in the RKG (1.3) for $0 < \varepsilon \leq 1$.

4.1. Accuracy test.

Here we test the convergence of the proposed methods. We take a 2D example in (1.3), i.e. $d = 2$, $\mathbf{x} = (x, y)$,

$$\Omega = 1,\ \lambda = 0.5,\ V(\mathbf{x}) = \frac{|\mathbf{x}|^2}{2}\mathrm{e}^{-|\mathbf{x}|^2},\ \psi_0(\mathbf{x}) = \mathrm{e}^{-2x^2-1.5y^2}\frac{x+iy}{|\mathbf{x}|^2+1},\ \psi_1(\mathbf{x}) = \frac{i\psi_0(\mathbf{x})}{\varepsilon^2}, \tag{4.1}$$

and solve the problem till $T = \pi/4$.

Accuracy confirmation of SIFS. In polar coordinates, the computational domain is chosen as the disk of radius $R_0 = 10$ centered at the origin. We shall test the temporal and spatial accuracy (in both r and θ-directions) for different ε. The benchmark solution is obtained with fine mesh $\Delta t = T/2^{14}$, $N_r = 2048$ in the r-direction and $N_\theta = 128$ in the θ-direction. For the temporal error test, we fix grid points $N_r = 2048$ and $N_\theta = 128$ such that errors coming from the r and θ are negligible, and we compute the errors with different number of time grids $N = T/\Delta t$. The relative maximum error in Ψ and the corresponding convergence rates are presented in Tab. 2. We see that under a fixed N, the error of SIFS increases dramatically as ε decreases and the method loses its efficiency in the limit regime.

To confirm the spatial accuracy in the r-direction, we choose $N_\theta = 128, \Delta t = T/2^{14}$ such that errors from θ and Δt are negligible, and compute the relative maximum for different N_r. Fig. 2 (the second figure) displays the spatial error in r-direction, together with convergence rates, for different ε. The spectral accuracy in the θ-direction is confirmed by Fig. 2, where we use the same fine mesh and time step as $N_r = 2048, \Delta t = T/2^{14}$ for different ε.

TABLE 2. Second order convergence confirmation of SIFS in Δt under different ε.

	$N = 128$	$N * 2$	$N * 2^2$	$N * 2^3$	$N * 2^4$	$N * 2^5$
$\varepsilon = 1$	6.16E-3	1.56E-3	3.93E-4	9.84E-5	2.44E-5	5.81E-6
rate	-	1.98	1.99	2.00	2.01	2.07
$\varepsilon = 1/2$	8.06E-2	2.05E-2	5.15E-3	1.29E-3	3.19E-4	7.61E-5
rate	-	1.98	1.99	2.00	2.01	2.07
$\varepsilon = 1/4$	8.51E-1	2.47E-1	6.27E-2	1.57E-2	3.88E-3	9.26E-4
rate	-	1.78	1.98	2.00	2.01	2.07
$\varepsilon = 1/8$	5.77	8.78E-1	1.66	4.66E-1	1.16E-1	2.78E-2
rate	-	2.72	-0.92	1.83	2.00	2.07

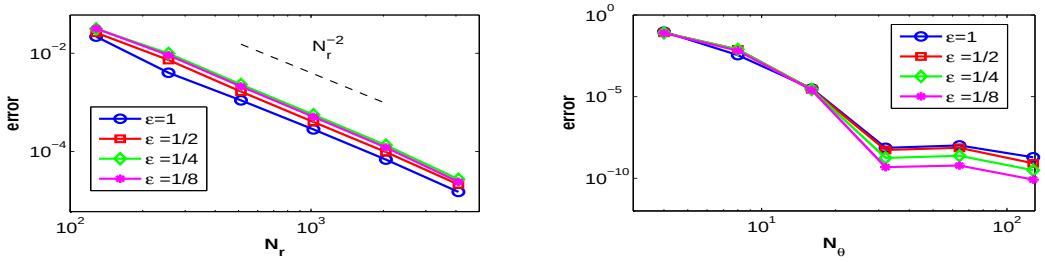

FIGURE 2. Error of SIFS with respect to the number of temporal grids N_r and N_θ under different ε.

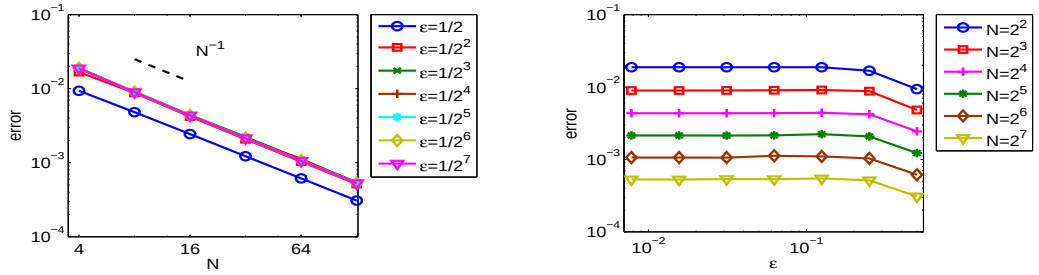

FIGURE 3. Error of EI with respect to the number of temporal grids N under different ε.

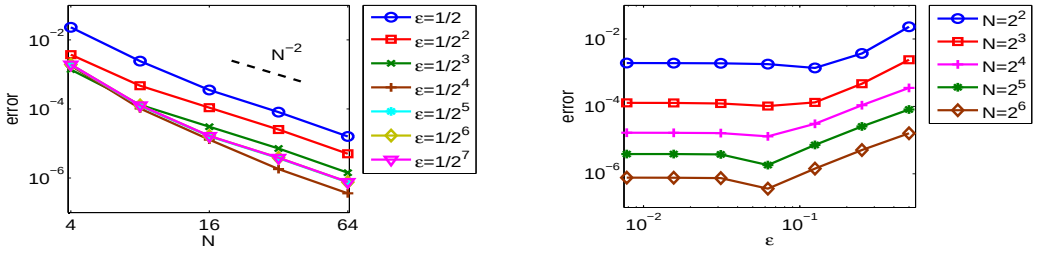

FIGURE 4. Error of MRC with respect to the number of (macro) temporal grids N under different ε.

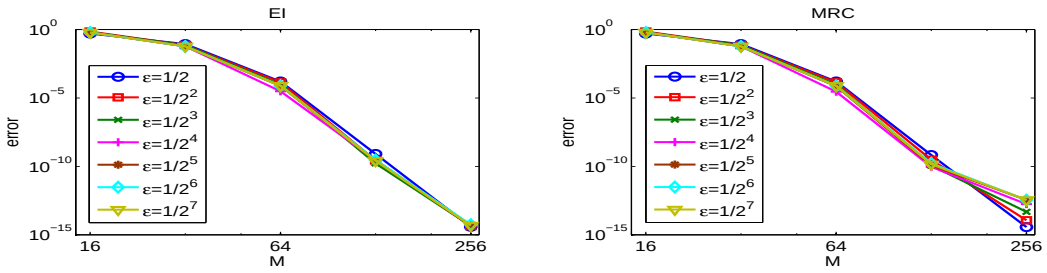

FIGURE 5. Error of EI and MRC with respect to the number of spatial grids (in x or y) M under different ε.

Uniform accuracy confirmation of MRC and EI. For the MRC and EI methods in Cartesian coordinates, we take the truncated square domain as $I = (-8, 8)^2$. To study the temporal error of the two methods, we fix the number of grids $M = 256$ to discretize the space x or y-direction (i.e. $\Delta x = \Delta y = 1/16$) such that the discretization error is negligible. The error of EI with respect to the number of grids $N = T/\Delta t$ in time is shown in Fig. 3 under different ε, and the error of MRC with respect to N is shown Fig. 4. To study the spatial discrestization error of MRC and EI, we fix the number of the temporal grids $N = 512$ and plot the error with respect to M. The errors are shown in Fig. 5 under different ε.

From the numerical results, we see that the error of both EI and MRC converge in time and also in space uniformly for all $0 < \varepsilon \leq 1$. In particular, EI is uniformly first order accurate in time and MRC is uniformly second order with respect to the macro grids N. In space, MRC and EI are uniformly spectrally accurate. The uniform accuracy property of the schemes allow to use large time step which certainly increases the efficiency of simulations compared to the algorithm in polar coordinates.

4.2. **Vortices creation.** By taking a non-symmetric initial data with non-zero charge, vortices can be generated in the RKG (1.3), which obeys the relativistic Feynman relation [53, 28]. Here to simulate this phenomenon, we consider (1.3) in the relativistic regime, i.e. $\varepsilon = 1$. We take the initial values as

$$\Psi_0(\mathbf{x}) = \rho_0(\mathbf{x}) \mathrm{e}^{iN_0\theta}, \quad \Psi_1 = i\omega\Psi_0(\mathbf{x}),$$

with $\rho_0(\mathbf{x})$ as an anisotropic Gaussian, $N_0 \in \mathbb{N}^+$ and $\omega \in \mathbb{R}^+$. We apply the SIFS method to solve the RKG (1.3).

The numerical simulation is carried out on a disk of radius $R_0 = 10$ with $N_\theta = 128, N_r = 2048$ and $\Delta t = 10^{-4}$ for $\Omega = 1, \lambda = 2$ under potential $V = r^2$. The initial anisotropic distribution is chosen as $\rho_0 = e^{-2x^2-1.5y^2}$ with $\omega = 1$ and $N_0 = 2$ or 3. In Fig. 6, we can see that clearly there are no vortices initially, but as time evolves, some vortices will be created during the dynamics. The maximum number of vortices that could be generated equals to N_0.

4.3. **Dynamics and interactions.**

Example 4.1. *(Relativistic effect on the bound state)* We take the bound state $z_\pm$ of the RNLS (2.7) obtained in Fig. 1 and input it as the initial value of the RKG (1.4) as

$$\psi_0(\mathbf{x}) = z_+(\mathbf{x}) + \overline{z}_-(\mathbf{x}), \quad \psi_1(\mathbf{x}) = i(z_+(\mathbf{x}) - \overline{z}_-(\mathbf{x})),$$

which is asymptotically consistent with expansion (2.1) as $\varepsilon \to 0$. The other computational setups for RKG (1.3) are the same as for the bound state, i.e. $\lambda = 50$, $V = \frac{1}{2}(x^2 + y^2)$ and $\Omega = 0.9$. We solve the RKG under $\varepsilon = 1$ and $\varepsilon = 1/8$ by MRC and the solution at different time is shown in Fig. 7. From the results we see that when $\varepsilon = 1$, the relativistic effect does a strong modification to the vortices pattern as time evolves. As ε becomes small, the vortices pattern maintains well in the dynamics.

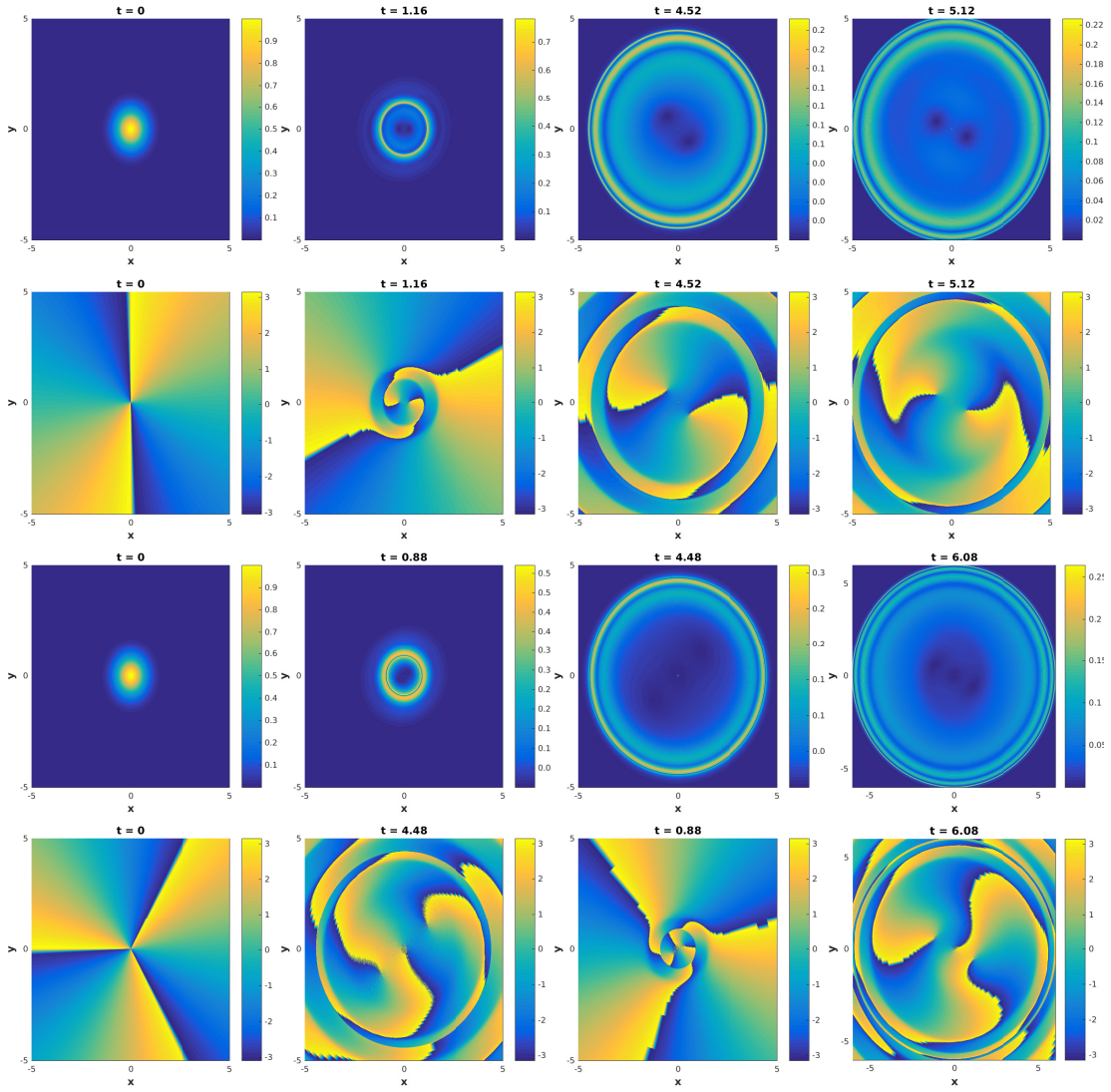

FIGURE 6. Contour plot of $|\Psi(t)|$ and $\mathrm{Arg}(\Psi)(t)$ at different times with $N_0 = 2$ (top two rows) and $N_0 = 3$ (last two rows).

Example 4.2. *(Interaction of vortex pairs and dipoles)* We consider the interaction of two vortex pairs and dipoles in the RKG (1.3) in two dimensions. We take the parameters in the equation as

$$\Omega = 0.5, \quad \lambda = 10,$$

and the initial data as two vortex pairs:

$$\psi_0(\mathbf{x}) = \psi_1(\mathbf{x}) = (x - c_0 + iy)(x + c_0 + iy)(x + i(y - c_0))(x + i(y + c_0))\mathrm{e}^{-(x^2+y^2)/2},$$

with $c_0 = 1.32$. Considering the symmetric potential case

$$V(\mathbf{x}) = \frac{1}{2}(x^2 + y^2),$$

we solve the problem under different ε by MRC in the Lagrangian coordinates on domain $(-32, 32)^2$ till $t = \pi$. In Fig. 8, the solution $|\Psi(\mathbf{x}, t)|$ and $\mathrm{Arg}(\Psi(\mathbf{x}, t))$ are plotted at different time t under $\varepsilon = 1, 1/4$. The time evolutions of the numerical energy $E^n \approx E(t_n)$ and the numerical charge

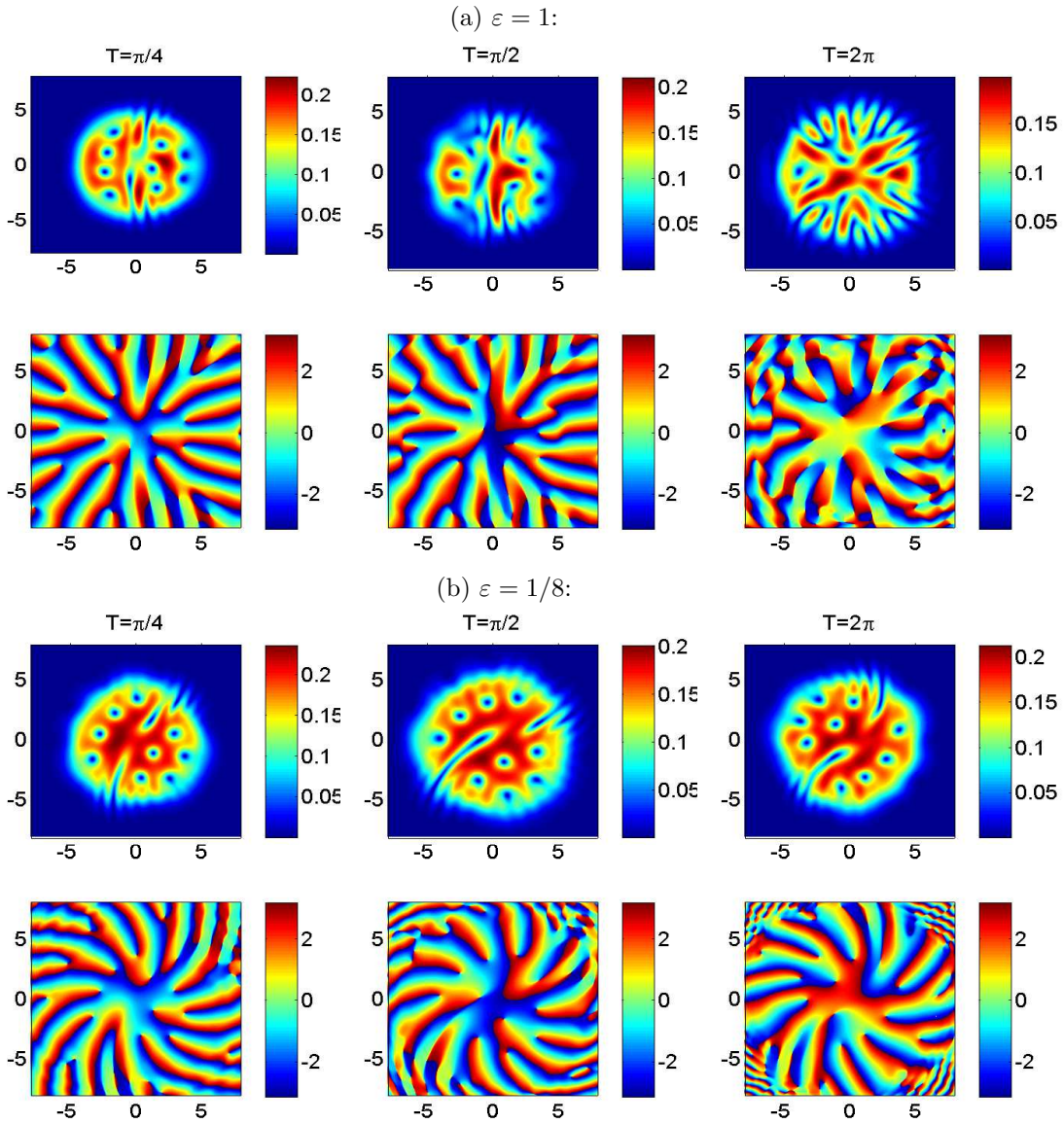

FIGURE 7. Contour plot of $|\Psi|$ and $\mathrm{Arg}(\Psi)$ in example 4.1 under: (a) $\varepsilon = 1$; (b) $\varepsilon = 1/8$.

$Q^n \approx Q(t_n)$ given by the scheme during the simulation are shown in Fig. 9. For an non-symmetric potential case,

$$V(\mathbf{x}) = 0.5x^2 + 1.5y^2,$$

we solve the problem by EI and the results under $\varepsilon = 1/4$ are shown in Fig. 10.

5. Conclusion

We considered the rotating nonlinear Klein-Gordon (RKG) equation which contains first order and second order angular momentum operator terms for modelling a rotating galaxy in cosmology. We showed that in the non-relativistic limit regime, RKG formally converges to a coupled rotating nonlinear Schrödinger (RNLS) model. In fact, the limit RNLS model describes the dynamics of the rotating two-component Bose-Einstein Condensates. We discussed and compared the RKG model with the RNLS. We then presented numerical algorithms for efficiently solving the RKG in polar coordinates or in Cartesian coordinates. In particular, we applied a rotating Lagrangian coordinates

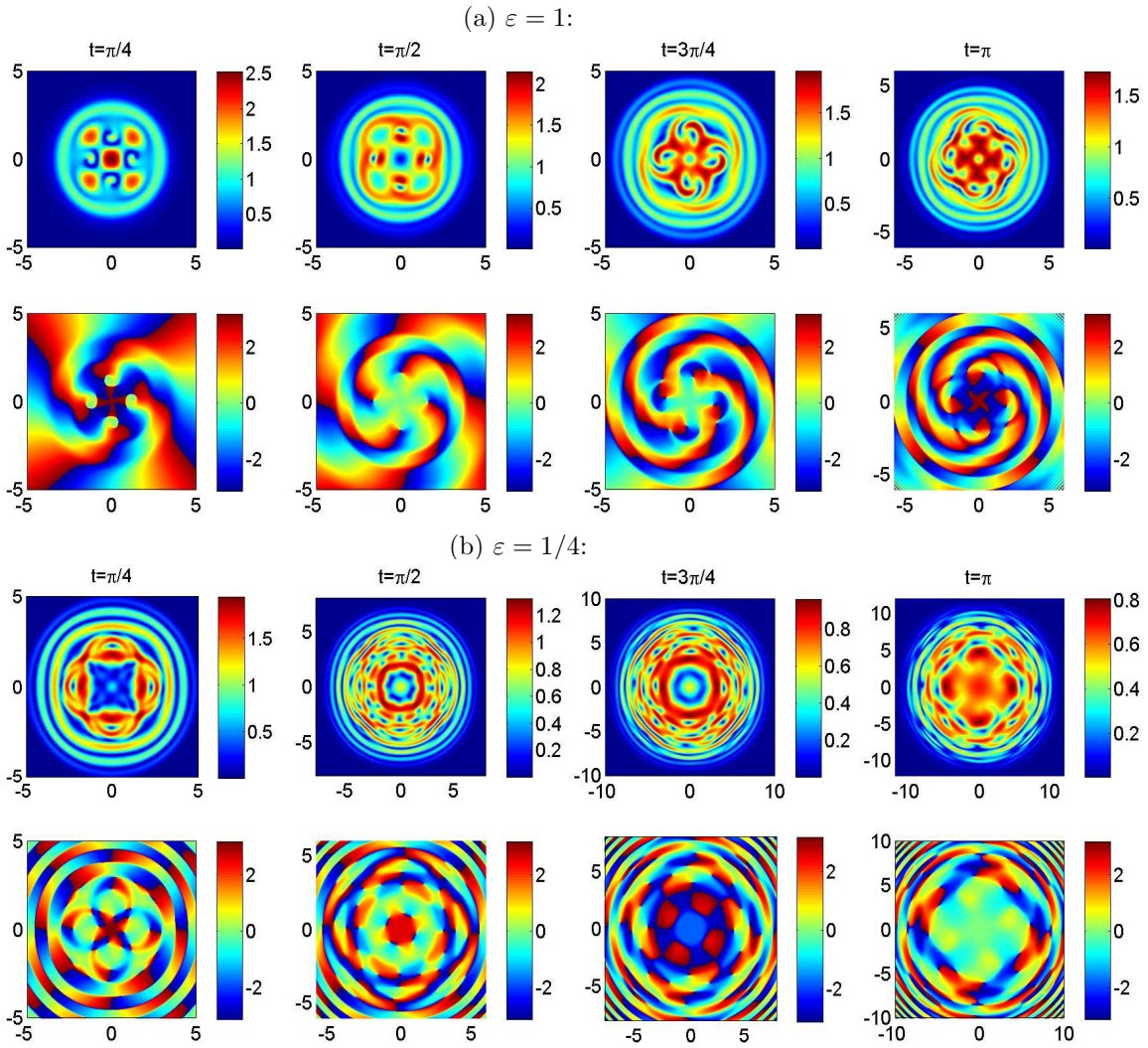

FIGURE 8. Contour plot of $|\Psi|$ and $\mathrm{Arg}(\Psi)$ in example 4.2 with symmetric potential under: (a) $\varepsilon = 1$; (b) $\varepsilon = 1/4$.

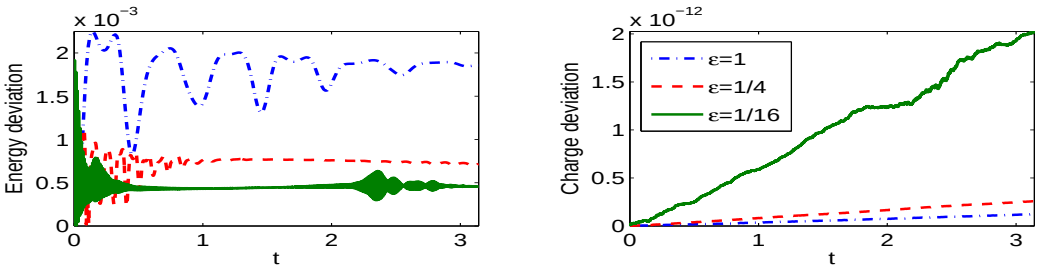

FIGURE 9. Deviation of the energy (1.5) and the charge (1.6) of the computation by MRC in Fig. 8: $|E^n - E(0)|/|E(0)|$ and $|Q^n - Q(0)|/|Q(0)|$.

transform which eliminates both angular terms in the RKG, so that the multiscale strategies were further applied to get uniform accurate numerical schemes for solving the RKG in the non-relativistic

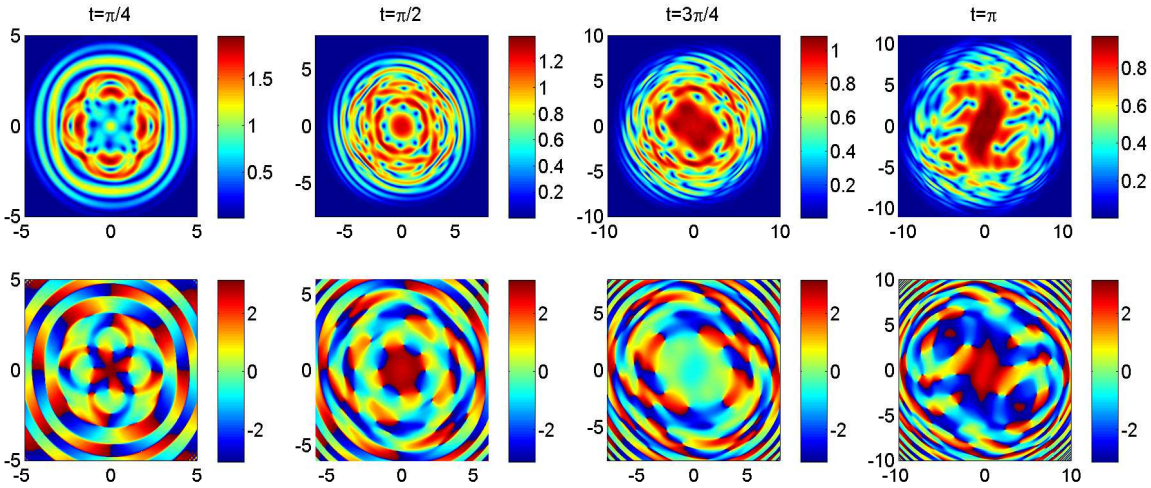

FIGURE 10. Contour plot of $|\Psi|$ and $\mathrm{Arg}(\Psi)$ in example 4.2 with non-symmetric potential at different t under $\varepsilon = 1/4$.

limit regime. With the proposed methods, we studied the quantized vortices dynamics in RKG from relativistic regime to the non-relativistic regime. Simulation results were presented in the end.

ACKNOWLEDGEMENTS

The work is dedicated to the memory of Prof. Kerson Huang. X. Zhao is supported by the French ANR project MOONRISE ANR-14-CE23-0007-01. Y. Zhang was supported by the Austrian Science Foundation (FWF) via his Schrödinger Fellowship J3784-N32, and under grant No. F41 (SFB "VICOM") and grant No. F65 (SFB "Complexity in PDEs"). Also support from the Wiener Wissenschafts und TechnologieFonds (WWTF) project No. MA16-066 ("SEQUEX") is acknowledged. We thank Dr. Chi Xiong for helpful discussions.

REFERENCES

[1] P. Allmer , N.J. Mauser, Semiclassical limit of the Klein-Gordon equation, (2018) manuscript.
[2] W. Bao, Y. Cai, Mathematical theory and numerical methods for Bose-Einstein condensation, Kinetic and Related Models 6 (2013) pp.1-135.
[3] W. Bao, Y. Cai, X. Zhao, A uniformly accurate multiscale time integrator pseudospectral method for the Klein-Gordon equation in the nonrelativistic limit regime, SIAM J. Numer. Anal. 52 (2014) pp.2488-2511.
[4] W. Bao, X. Dong, Analysis and comparison of numerical methods for the Klein-Gordon equation in the non-relativistic limit regime, Numer. Math. 120 (2012) pp.189-229.
[5] W. Bao, X. Dong, X. Zhao, Uniformly accurate multiscale time integrators for highly oscillatory second order differential equations, J. Math. Study 47 (2014) pp.111-150.
[6] W. Bao, Q. Du, Y. Zhang, Dynamics of rotating Bose-Einstein condensates and its efficient and accurate numerical computation, SIAM J. Appl. Math. 66 (2006) pp.758-786.
[7] W. Bao, H. Li, J. Shen, A generalized-Laguerre-Fourier-Hermite pseudospectral method for computing the dynamics of rotating Bose-Einstein condensates, SIAM J. Sci. Comput. 31 (2009) pp.3685-3711.
[8] W. Bao, D. Marahrens, Q. Tang, Y. Zhang, A simple and efficient numerical method for computing the dynamics of rotating Bose–Einstein condensates via rotating Lagrangian coordinates, SIAM J. Sci. Comput. 35 (2013) pp.A2671-A2695.
[9] D.D. Bǎinov, E. Minchev, Nonexistence of global solutions of the initial-boundary value problem for the nonlinear Klein-Gordon equation, J. Math. Phys. 36 (1995) pp.756-762.
[10] W. Bao, Q. Tang, Numerical study of quantized vortex interaction in nonlinear Schrödinger equation on bounded domains, Multiscale Model. Simul. 12 (2014) pp.411-439.
[11] W. Bao, Q. Tang, Numerical study of quantized vortex interaction in the Ginzburg-Landau equation on bounded domains, Comput. Phys. Comm. 14 (2013) pp.819-850.
[12] W. Bao, R. Zeng, Y. Zhang, Quantized vortex stability and interaction in the nonlinear wave equation, Physica D 237 (2008) pp.2391-2410

[13] S. Baumstark, E. Faou, K. Schratz, Uniformly accurate exponential-type integrators for Klein-Gordon equations with asymptotic convergence to the classical NLS splitting, Math. Comp. 87 (2018) pp.1227-1254.
[14] P. Bechouche, N.J. Mauser, S. Selberg, Nonrelativistic limit of Klein-Gordon Maxwell to Schrödinger-Poisson, Amer. J. Math. 126 (2004) pp.31-64.
[15] V.B. Bezerra, H.S. Vieira, A.A. Costa, The Klein-Gordon equation in the spacetime of a charged and rotating black hole, Class. Quantum Grav. 31 (2014) pp.045003.
[16] J.D. Bjorken, S. Drell, Relativistic Quantum Fields, McGraw-Hill (1965).
[17] Ph. Chartier, N. Crouseilles, M. Lemou, F. Méhats, Uniformly accurate numerical schemes for highly oscillatory Klein-Gordon and nonlinear Schrödinger equations, Numer. Math. 129 (2015) pp.211-250.
[18] Ph. Chartier, N. Crouseilles, X. Zhao, Numerical methods for the two-dimensional Vlasov-Poisson equation in the finite Larmor radius approximation regime, J. Comput. Phys. 375 (2018) pp.619-640.
[19] Ph. Chartier, J. Makazaga, A. Murua, G. Vilmart, Multi-revolution composition methods for highly oscillatory differential equations, Numer. Math. 128 (2014) pp.167-192.
[20] Ph. Chartier, F. Méhats, M. Thalhammer, Y. Zhang, Convergence analysis of multi-revolution composition time-splitting pseudo-spectral methods for highly oscillatory differential equations of Schrödinger equations, ESAIM:M2AN 51 (2017) pp.1859-1882.
[21] S.K. Chakrabarti, P.R. Giri, K.S. Gupta, Normal mode analysis for scalar fields in BTZ black hole background, Eur. Phys. J C 60 (2009) pp.169-173.
[22] X. Dong, Z. Xu, X. Zhao, On time-splitting pseudospectral discretization for nonlinear Klein-Gordon equation in nonrelativistic limit regime, Commun. Comput. Phys. 16 (2014) pp.440-466.
[23] S. Detweiler, Klein-Gordon equation and rotating black holes, Phys. Rev. D 22 (1980) pp.2323.
[24] E. Faou, K. Schratz, Asympotic preserving schemes for the Klein-Gordon equation in the non-relativistic limit regime, Numer. Math. 126 (2014) pp.441-469.
[25] H.R.C. Ferreira, C.A.R. Herdeiro, Stationary scalar clouds around a BTZ black hole, Phys. Lett. B 773 (2017) pp.129-134.
[26] V.L. Ginzburg, L.D. Landau, Toward the superconductivity theory, Zh. Eksp. Teor. Fiz. 20 (1950) pp. 1064.
[27] M. Good, C. Xiong, A. Chua, K. Huang, Geometric creation of quantum vorticity, New J. Phys. 18 (2016) pp.113018.
[28] Y. Guo, X. Liu, C. Xiong, X. Xu, C. Fu, Towards high-quality visualization of superfluid vortices, IEEE Trans. Vis. Comput. Graph. 24 (2018) pp. 2440-2455.
[29] D.S. Hall, M.R. Matthews, J.R. Ensher, C.E. Wieman, E.A. Cornell, Dynamics of component separation in a binary mixture of Bose-Einstein condensates, Phys. Rev. Lett. 81 (1998) pp.1539-1542.
[30] T.L. Ho, V.B. Shenoy, Binary mixtures of Bose condensates of alkali atoms, Phys. Rev. Lett. 77 (1996) pp.327-3279.
[31] K. Huang, A Superfluid Universe, World Scientific, 2016. (ISBN 9813148454).
[32] K. Huang, C. Xiong, X. Zhao, Scalar-field theory of dark matter, Internat. J. Modern Phys. A 29 (2013) pp.1450074.
[33] K. Huang, H. Low, R. Tung, Scalar Field Cosmology II: Superfluidity, Quantum Turbulence, and Inflation, Internat. J. Modern Phys. A 27 (2012) pp.1250154.
[34] B. Li, Z. Zhang, A new approach for numerical simulation of the time-dependent Ginzburg-Landau equations, J. Comput. Phys. 303 (2015) pp. 238-250.
[35] J. Jin, S. Zhang, W. Han, Z. Wei, The ground states and spin textures of rotating two-component Bose-Einstein condensates in an annular trap, J. Phys. B: At. Mol. Opt. Phys. 46 (2013) pp.075302.
[36] K. Kasamatsu, M. Tsubota, M. Ueda, Vortex phase diagram in rotating two-component Bose-Einstein condensates, Phys. Rev. Lett. 91 (2003) pp.150406.
[37] I.M. Khalatnikov, An Introduction to the Theory of Superfluidity, Addison-Wesley, New York, 1989.
[38] M.C. Lai, W.W. Lin, W. Wang, A fast spectral/difference method without pole conditions for Poisson-type equations in cylindrical and spherical geometries, IMA J. Numer. Anal. 22 (2002) pp.537-548.
[39] H.B. Low, C. Xiong, Fantasia of a Superfluid Universe-In Memory of Kerson Huang, arXiv:1612.01347.
[40] N.J. Mauser, Y. Zhang, Exact artificial boundary condition for the Poisson equation in the simulation of the 2D Schrödinger-Poisson system, Commun. Comput. Phys. 16 (2014) pp.764-780.
[41] J. Ming, Q. Tang, Y. Zhang, An efficient spectral method for computing dynamics of rotating two-component Bose-Einstein condensates via coordinate transformation, J. Comput. Phys. 258 (2014) pp.538-554.
[42] S. Machihara, K. Nakanishi, T. Ozawa, Nonrelativistic limit in the energy space for nonlinear Klein-Gordon equations, Math. Ann. 322 (2002) pp.603-621.
[43] N. Masmoudi, K. Nakanishi, From nonlinear Klein-Gordon equation to a system of coupled nonlinear Schrödinger equations, Math. Ann. 324 (2002) pp.359-389.
[44] N.J. Mauser, Semi-relativistic approximations of the Dirac equation: first and second order corrections, Transp. Theor. Stat. Phys. 29 (2000) pp.122-137.
[45] N.J. Mauser, S. Selberg, Convergence of the Dirac-Maxwell system to the Vlasov-Poisson system, Comm. PDE 32 (3) (2007) pp.503-524
[46] C.J. Myatt, E.A. Burt, R.W. Ghrist, E.A. Cornell, G. E. Wieman, Production of two overlapping Bose-Einstein condensates by sympathetic cooling, Phys. Rev. Lett. 78 (1997) pp. 586-589.

[47] B. Najman, The nonrelativistic limit of the nonlinear Klein-Gordon equation, Nonlinear Anal. 15 (1990) pp.217-228.
[48] B. Pourhassan, The Klein-Gordon equation of a rotating charged hairy black hole in (2+1) dimensions, Modern Phys. Lett. A 31 (2016) pp.1650057.
[49] D.J. Rowan, G. Stephenson, The Klein-Gordon equation in a Kerr-Newman background space, J. Phys. A: Math. Gen. 10 (1077) pp.15-23.
[50] Q. Tang, Y. Zhang, N.J. Mauser, A robust and efficient numerical method to compute the dynamics of the rotating two-component dipolar Bose-Einstein condensates, Comput. Phys. Comm. 219 (2017) pp.223-235.
[51] M. Tsubota, K. Kasamatsu, M. Ueda, Vortex lattice formation in a rotating Bose-Einstein condensate, Phys. Rev. A 65 (2002) pp. 023603.
[52] P. Valtancoli, Scalar field conformally coupled to a charged BTZ black hole, Ann. Physics 369 (2016) pp. 161-167.
[53] C. Xiong, M. Good, Y. Guo, X. Liu, K. Huang, Relativistic superfluidity and vorticity from the nonlinear Klein-Gordon equation, Phys. Rev. D 90 (2014) pp.125019.
[54] C. Xiong, K. Huang, Relativistic two-fluid hydrodynamics with quantized vorticity from the nonlinear Klein-Gordon equation, arXiv:1612.09248.
[55] O. Waldron, R. A.Van Gorder, A nonlinear Klein-Gordon equation for relativistic superfluidity, Phys. Scripta 92 (2017), pp.105001.
[56] S. Weinberg, The Quantum Theory of Fields, Volume 1: Foundations. Cambridge University Press, 1995.
[57] E. Witten, Superconducting strings, Nucl. Phys. B 249 (1985), pp.557-592.
[58] W.H. Zurek, Cosmological experiments in superfluid helium? Nature 317 (1985) pp.505-508.
[59] Y. Zhang, W. Bao and H. Li, Dynamics of rotating two-component Bose-Einstein condensates and its efficient computation, Phys. D 234 (2007) pp.49-69.

N. Mauser: Wolfgang Pauli Institute c/o Fak. Mathematik, Univ. Wien, Oskar-Morgenstern-Platz 1, A-1090, Vienna.
E-mail address: norbert.mauser@univie.ac.at
URL: https://www.wpi.ac.at/director.html

Y. Zhang: Center for Applied Mathematics,Tianjin University,Tianjin 300072,China
E-mail address: Zhang_Yong@tju.edu.cn
URL: http://cam.tju.edu.cn/~yzhang/

X. Zhao: Univ. Rennes, INRIA-MINGuS, CNRS, IRMAR-UMR 6625, F-35000 Rennes, France
E-mail address: zhxfnus@gmail.com